Scholars' Mine

Masters Theses   Student Theses and Dissertations

1967

Compressive creep of high alumina refractories

Vernon Lee Burdick

Follow this and additional works at: https://scholarsmine.mst.edu/masters_theses

Part of the Ceramic Materials Commons

Department:

Recommended Citation

Burdick, Vernon Lee, "Compressive creep of high alumina refractories" (1967). *Masters Theses*. 5162.
https://scholarsmine.mst.edu/masters_theses/5162

COMPRESSIVE CREEP OF HIGH ALUMINA REFRACTORIES

———————

A Dissertation

Presented to

the Faculty of the Graduate School

University of Missouri at Rolla

———————

In Partial Fulfillment

of the Requirements for the Degree

Doctor of Philosophy

———————

by

Vernon Lee Burdick

June 1967   132103

ABSTRACT

The deformation of refractory materials consisting of
90% sintered or fused alumina plus 10% silica was measured
at temperatures from 1450 to 1515°C and a compressive stress
of 100 psi. Creep rates and activation energies were deter-
mined from the steady state portion of deformation vs. time
data and correlated with the mineralogical composition.
Supplemental measurements included x-ray diffraction,
electron probe microanalysis, apparent porosity and tensile
strength.

Conditions having an important effect upon the mineral-
ogical composition were: (1) duration of heat treatment,
(2) amount of sodium oxide impurity, and (3) reactivity of
the alumina grain. Prolonged heat treatment and sodium oxide
impurity enhanced mullite formation, thus lowering creep
rates.

The activation energies ranged from 75 kcal/mole for
samples containing sintered alumina doped with 0.5% sodium
oxide, to 140-150 kcal/mole for regular sintered or fused
alumina. The magnitude of the activation energy was approx-
imately proportional to the mullite content.

Vernon L. Burdick

ACKNOWLEDGMENT

TABLE OF CONTENTS

LIST OF TABLES

TABLE NUMBER

LIST OF FIGURES

FIGURE NUMBER

APPENDIX

I INTRODUCTION

The high temperature technology of the glass, cement and steel industries requires refractories of exceptionally good chemical durability and mechanical strength. Refractories containing more than 50% alumina meet the requirements economically where fireclay refractories have failed. The rapid growth in the demand for high alumina refractories is illustrated by the 107% increase in shipments over the last decade.[1]

In considering the properties of aluminosilicate refractories, the alumina-silica phase diagram (Figure 1) is usually employed with impurities being neglected. Between 10 and 70% alumina, where the first liquid appears at 1595°C, the amount of liquid at a given temperature decreases as the alumina content increases. Concurrently, the liquidus temperature increases in this composition range. In compositions containing more than 70% alumina where mullite and α alumina are the stable solid phases at equilibrium, the eutectic temperature is 1840°C. With increasing alumina content the amount of liquid decreases and the liquidus temperature increases until 100% alumina is attained. Based on these observations, it is usually concluded that the ability to withstand high temperatures increases with increasing alumina content. Although this conclusion is valid for the pure two component system, it does not necessarily apply to a more practical system containing
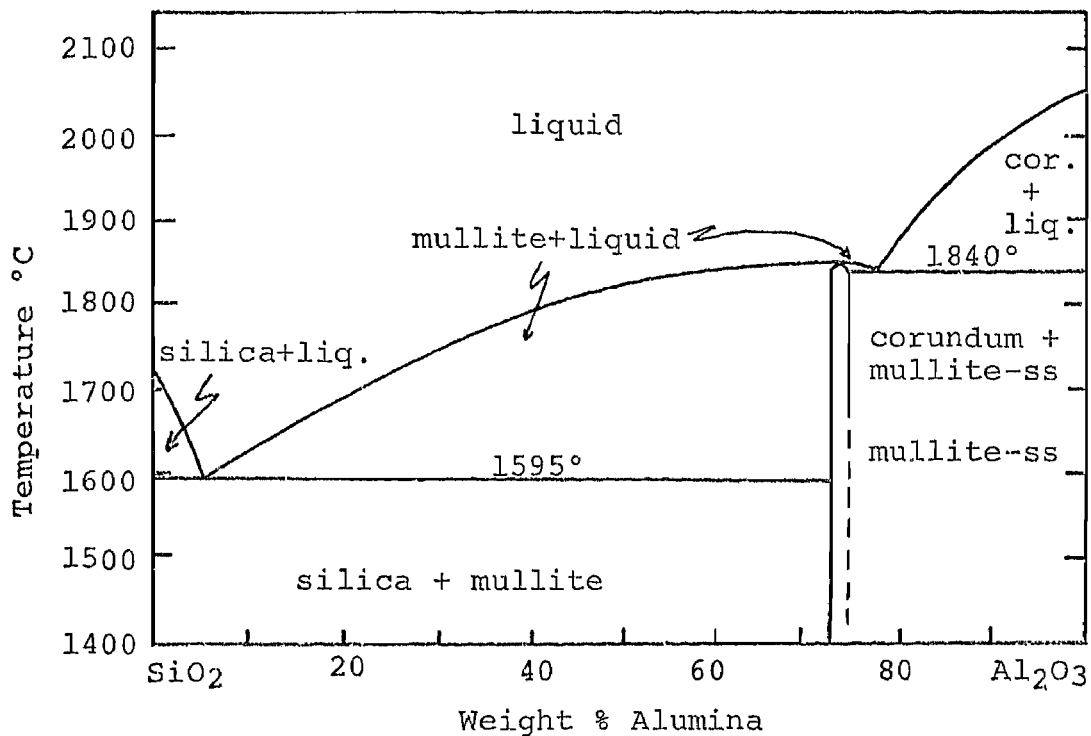
Figure 1.   The System Al_2O_3–SiO_2*

---

* S. Aramaki and R. Roy, "Revised Phase Diagram for the
  System Al_2O_3–SiO_2", J. Am. Ceram. Soc. <u>45</u> (5) 229–42
  (1962)

Note: The following chemical nomenclature is used in
        this thesis.

        Silica (silicon dioxide) = SiO_2
        Alumina (aluminum oxide) = Al_2O_3
        Soda (sodium oxide) = Na_2O

impurities, pores, and non-equilibrium phases. These devia-tions from the ideal chemical system are introduced by process or materials variables and are expected to influence the performance of refractories during service. The proper-ties affected include mechanical strength and resistance to deformation under load at high temperatures.

One of the important design limitations of refractories is their resistance to deformation under load at high temperatures. This property, often referred to as creep resistance, is affected by chemical composition, mineralog-ical composition, firing treatment and porosity.

The purpose of the research reported herein was to compare the creep behavior of 90% alumina refractories composed of either sintered or fused alumina plus silica. The nature of the alumina grain and the bonding matrix were of special interest. The mechanism of the creep process and its relation to microstructure and phase composition was also studied.

As in most thermally activated processes, the activation energy for creep is often characteristic of the creep mechanism. One method of identifying the creep mechanism is to measure the activation energy for the process. This method can only be used if the activation energy for various mechanisms is known from previous work. In the present study, the activation energy for creep in 90% alumina samples was compared to previously determined values for the activa-tion energy of creep in mullite and fireclay refractories.

The nature of the alumina grain and the bonding matrix was determined from microstructure studies, X-ray diffraction phase studies and electron probe microanalysis. This information was used in conjunction with creep data to further describe the creep behavior of samples containing sintered or fused alimina.

II LITERATURE REVIEW

Creep is defined as the deformation of a solid substance under constant stress. It constitutes a flow or rearrangement of matter in a direction so as to relieve the imposed stress. Several important variables which affect this flow process are time, temperature, stress and the nature of the material.

A. Time Dependence of Creep

The time dependence of creep, i.e. creep rate, is similar for a variety of solids including metals, polymers and ceramics. This behavior is often illustrated by a typical creep curve such as the one shown in Figure 2. This curve can be divided into four sections[2]:   (1) an instantaneous extension; (2) a primary stage of decreasing rate; (3) a secondary stage of steady state creep; and (4) a tertiary stage of accelerating creep rate leading to failure.

A large number of equations have been derived to describe the time dependence of creep. While these may be valid expressions for specific materials under given test conditions, their empirical nature precludes an interpretation of creep phenomena based on real physical models. Kennedy[2] reviewed the most successful creep-time expressions and suggests that the equation

$$\varepsilon = a \log t + bt^n + ct \qquad n \cong 1/3 \qquad\qquad (1)$$
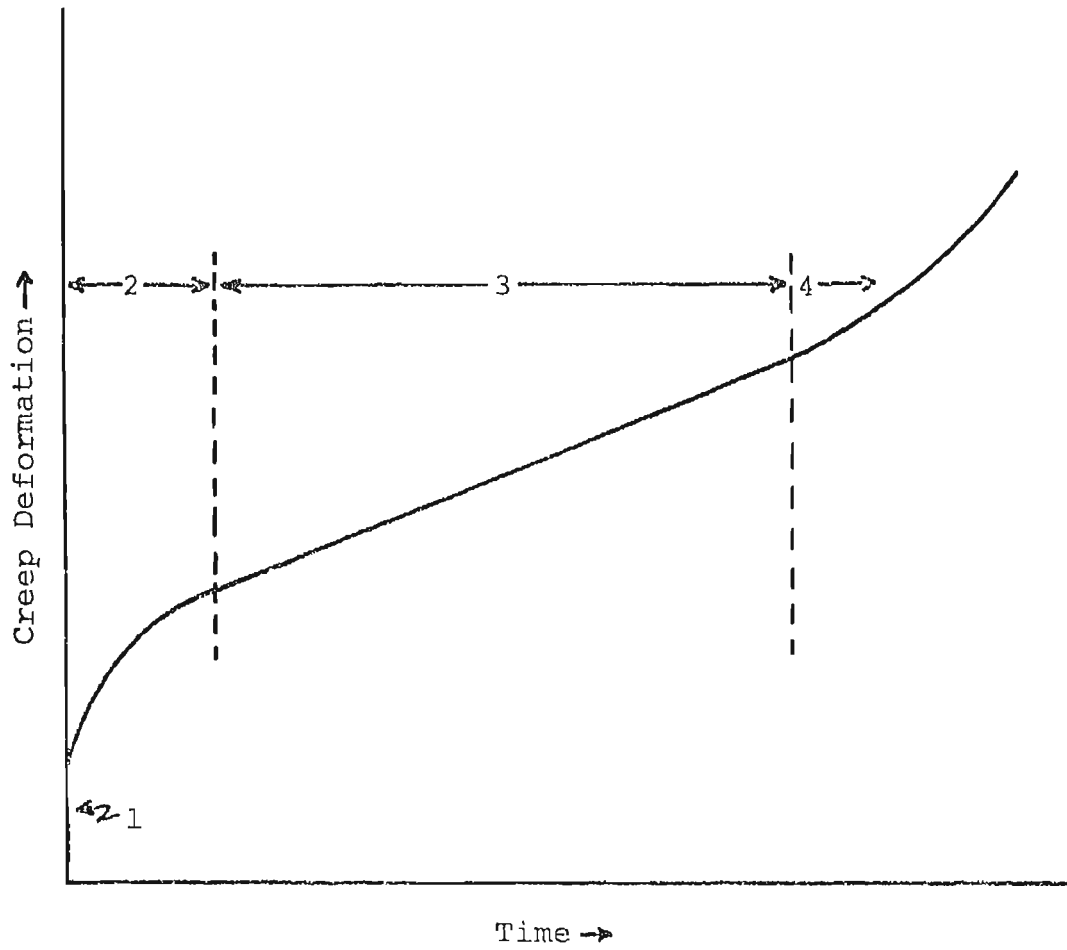
Figure 2.   Typical Creep Curve at Constant Stress
            and Temperature

where: ε = strain

a, b, c, = constants

t = time

proposed by Wyatt[3] is the best empirical relationship at present.

B.   Temperature and Stress Dependence of Creep

According to Dorn[4] the creep process is thermally activated. If thermal activation did not occur, the strain obtained at a given temperature would be only stress dependent. Thus, the time dependent creep phenomena are stimulated by continuous thermal excitation.

The temperature dependence of the creep rate is best described using rate process theory as outlined by Dorn[4] for metals, Gibbs and Eyring[5] for ceramics ,and applied by Hulse and Pask[6] to fireclay refractories. This theory is outlined in detail in Appendix A. According to this theory, the deformation of solid substances constitutes a movement of matter. This movement is pictured as a migration of density fluctuations within the material. Admittedly, these fluctuations having been introduced into the material at high temperature may vary in type but regardless of type, each fluctuation has an equilibrium position at a potential energy minimum[5]. The microstructural features of the material determine the potential energy surfaces limiting the motion of the fluctuations. When an external force is applied to the material, the potential energy surfaces are altered

thereby shifting the equilibrium positions slightly. With the passage of time there is a net migration of fluctuations over their barriers in a direction to relieve stress. The expression for creep rate as a function of stress and temperature is given as[5]:

$$S = (2K\delta/L)(\kappa T/h)\exp(-F/RT)\operatorname{Sinh}(b\sigma/RT) \qquad (2)$$

where: S = creep rate

K = transmission coefficient

κ = Boltzman's constant

T = absolute temperature

h = Plank's constant

F = activation energy

R = gas constant

σ = stress

b = constant

δ = stress axial component of one jump

L = distance between flow units

When creep rates are measured at constant stress and constant temperatures the equation becomes[6]:

$$S = Af(s)f(\sigma)\exp(-F/RT) \qquad (3)$$

where: A = constant

$f(s)$ = some function of creep structure

$f(\sigma)$ = some function of stress

Thus, the experimental activation energy for creep is calculated from the slope of a graph of the natural logarithm of the creep rate vs. the reciprocal of absolute temperature.

C. Creep Mechanisms

In single phase materials such as pure oxide ceramics, processes which can conceivably account for creep are:

1. Crystallographic slip

2. Dislocation climb

3. Grain boundary flow

4. Diffusion

Additionally, in a multiphase ceramic material such as a glass-crystal composite, a viscous or quasi-viscous flow of the glassy matrix can predominate in creep deformation. Practically all investigators agree that in most ceramic materials including aluminosilicate refractories the creep behavior is determined by the matrix material[6].

D. Creep of Refractory Materials

Creep measurements on refractories have emphasized the effects of chemical composition, mineralogical composition, porosity and firing treatment. Clements and Vyse[8] measured the compressive creep of some high alumina refractories at temperatures from 1450 to 1550°C. The samples containing from 40 to 96% alumina were taken from commercial refractories. Chemical composition, mineralogical composition, porosity and firing treatment were considered as the important factors governing the creep behavior. Statistical

treatment of these factors showed the creep to be substantially independent of alumina content, flux content and porosity. The firing treatment correlated strongly with the creep resistance. From an examination of the mineralogical composition and microstructure it was further concluded that the nature of the refractory grain and the bonding matrix were the most important factors determining the creep resistance of high alumina refractories. Fused mullite, calcined kyanite or sillimanite, and possibly corundum present as coarse grains showed good inherent creep resistance. Glassy bonds or poorly developed crystalline bonds were associated with high creep rates.

Similar conclusions concerning aluminosilicate refractories were reported by Wiechula and Roberts[9]. They investigated commercial refractories covering the entire aluminosilicate composition range. Torsional measurements of the shear modulus, shear strength and creep showed that a transition from almost complete rigidity to incipient plasticity occurred between 700 and 800°C irrespective of composition. This suggested that the same mechanism is responsible for the loss of rigidity in this temperature range. The observed decrease in creep rate with the increasing alumina content was consistent with the increased amount of mullite and corundum in the structure. The similarity between the reciprocal flow rate vs. temperature curves for the refractories and the viscosity curves for silica glass led to the conclusion that the glass in the refractories was

highly siliceous in character.

Chi. and Sosman[10] also studied an aluminosilicate material containing a glassy phase. The deformation of fired kaolinite samples containing about 40% alumina followed the relationship:

$$D = l_0[1-\exp(-t/\tau)]+kt \qquad (4)$$

where: D = percent deformation at time t

l_0 = percent initial deformation

τ = relaxation time

k = percent/minute, the steady flow rate

At temperatures between 1320 and 1400°C the deformation consisted of two parts; (1) deformation not linearly proportional to time, called initial flow and; (2) deformation proportional to time, called steady flow. It was concluded that the initial flow was an elastico-viscous deformation while the steady flow resulted from the viscous deformation of a glass or highly viscous liquid. The viscous flow was attributed to a silicate liquid. Small amounts (2 to 3%) of basic oxides present in the samples were considered sufficient for the formation of the silicate liquid.

In contrast, Hulse and Pask[6] raised some questions regarding the rate controlling process in the deformation of fireclay refractories. While the overall deformation depended upon the amount of glassy phase present, the temperature dependence of the creep rate indicated that in

some cases mullite was the rate controlling phase. In
specimens containing an interlocking mullite network, the
activation energy for creep was found to be 170 kcal/mole.
This value is close to the 177 kcal/mole activation energy
for a mullite refractory. The similarity in activation
energies suggested that mullite was the rate controlling
phase. Specimens showing poor mullite crystallization gave
an activation energy of 134 kcal/mole while specimens
wherein phase changes occurred during testing gave an acti-
vation energy higher than 170 kcal/mole.

III EXPERIMENTAL PROCEDURE

A. Sample Preparation

Samples were prepared using high soda fused alumina, low soda fused alumina, high soda sintered alumina, low soda sintered alumina and silica. A typical chemical analysis of each material was obtained from the supplier and is shown in Table I. The major chemical difference in the alumina materials is the soda content. Another significant difference is that the fused alumina grain is essentially mono-crystalline while the sintered alumina, having been sintered from a finely powdered material is polycrystalline. The maximum crystallite size in the sintered grain is about 150 microns.

The four types of alumina grain were separated into the size fractions 6 to 20 mesh, 20 to 60 mesh and -60 mesh by standard sieve techniques. It was desired to keep the size distribution of the -60 mesh material as nearly constant as possible for all materials. This was accomplished by separating the materials into closely graded sizes and reblending selected portions of each size fraction to give the desired size distribution. The final size distribution of the alumina aggregate is shown in Table II.

After sizing, the materials were mixed in a twin shell, dry blender in the proportions shown in Table III. Prior to pressing, 7 wt. % of a solution of 5 wt. % cellulose gum in water was added. Cylindrical samples 1 1/8 inches in

TABLE I

TYPICAL CHEMICAL ANALYSIS OF MATERIALS USED IN SAMPLE PREPARATION

OXIDE WEIGHT PERCENT

Oxide	Low Soda* Sintered Alumina	High Soda** Fused Alumina	High Soda*** Sintered Alumina	Low Soda† Fused Alumina	Silica††
SiO_2	0.06	0.05	0.06	0.06	99.8
Fe_2O_3	0.06	0.15	0.06	0.08	0.020
Na_2O	0.04	0.50	0.30	0.07	<0.005
TiO_2	0.01	0.02	0.01	0.008	0.014
Al_2O_3	99.5+	99.3	99.3+	99.8	0.050

* T-60 Tabular Alumina, Aluminum Company of America, Pittsburgh, Pennsylvania.

** 38 Alundum, Norton Company, Worcester, Massachusetts.

† DARA Fused Alumina, Alcan, Montreal, Quebec.

†† #390 Sil-Co-Sil, Ottawa Silica Company, Ottawa, Illinois.

*** Experimental Tabular Alumina, Aluminum Company of America, Pittsburgh, Pennsylvania.

TABLE II

SIEVE ANALYSIS OF MATERIALS USED IN SAMPLE PREPARATION

CUMULATIVE PERCENT FINER

U.S. Sieve Number	Low Soda Sintered Alumina	High Soda Fused Alumina	High Soda Sintered Alumina	Low Soda Fused Alumina	Silica
6	100.0	100.0	100.0	100.0	
10	81.6	86.9	77.8	75.7	
14	67.5	74.4	77.8	70.0	
20	55.9	56.1	55.6	55.3	
30	44.8	43.8	43.7	41.0	
40	38.6	35.6	37.4	35.7	
60	31.7	31.7	31.1	31.0	
100	21.0	19.2	22.5	22.2	
140	15.2	9.6	11.3	13.8	100.0
200	9.8	3.7	7.6	9.0	99.5
230	6.4	0.9	5.6	5.8	----
325	3.5	0.3	3.4	2.4	91.0

TABLE III

SAMPLE COMPOSITIONS

Sample	Composition	
F(0.5)	40% 6 to 20 mesh	
	22% 20 to 60 mesh	High Soda Fused Alumina
	28% -60 mesh	
	10% SiO_2	
S(0.04)	40% 6 to 20 mesh	
	22% 20 to 60 mesh	Low Soda Sintered Alumina
	28% -60 mesh	
	10% SiO_2	
S(0.5)	40% 6 to 20 mesh	
	22% 20 to 60 mesh	Low Soda Sintered Alumina
	28% -60 mesh	
	9.5% SiO_2	
	0.5% Na_2O added as Na_2CO_3	
S(0.3)	40% 6 to 20 mesh	
	22% 20 to 60 mesh	High Soda Sintered Alumina
	28% -60 mesh	
	10% SiO_2	
F(0.07)	40% 6 to 20 mesh	
	22% 20 to 60 mesh	Low Soda Sintered Alumina
	28% -60 mesh	
	10% SiO_2	

Numbers in parentheses indicate nominal soda content.

diameter and 1 inch long were pressed at 12,000 psi. The samples were dried at 110°C, heated in an electric furnace to 1530°C, and held at this temperature for either 3 or 7 hours. All forming processes were performed in an air atmosphere.

B. Creep Measurements

The creep was measured using a compressive loading apparatus shown schematically in Figure 3. The heating elements and load bearing members were silicon carbide. Deformation was measured at temperatures from 1450 to 1515°C under 100 psi load. The procedure employed was to raise the furnace temperature to the desired level, apply the load and record the deformation at specified times for a period of 24 to 36 hours. The creep rate was computed as the slope of the percent deformation vs. time curve in the steady state region. The slope was obtained by a linear least squares approximation. For the calculation of the activation energy for the creep process, the natural logarithm of the creep rate was plotted vs. the reciprocal of the absolute temperature. The slope of this curve multiplied by the gas constant yields the experimental activation energy for creep.

C. Supplementary Property Measurements

Firing shrinkage, bulk density and apparent porosity were measured by standard techniques. The tensile strength of the cylindrical samples was determined at room temperature using a diametral loading technique. The tensile
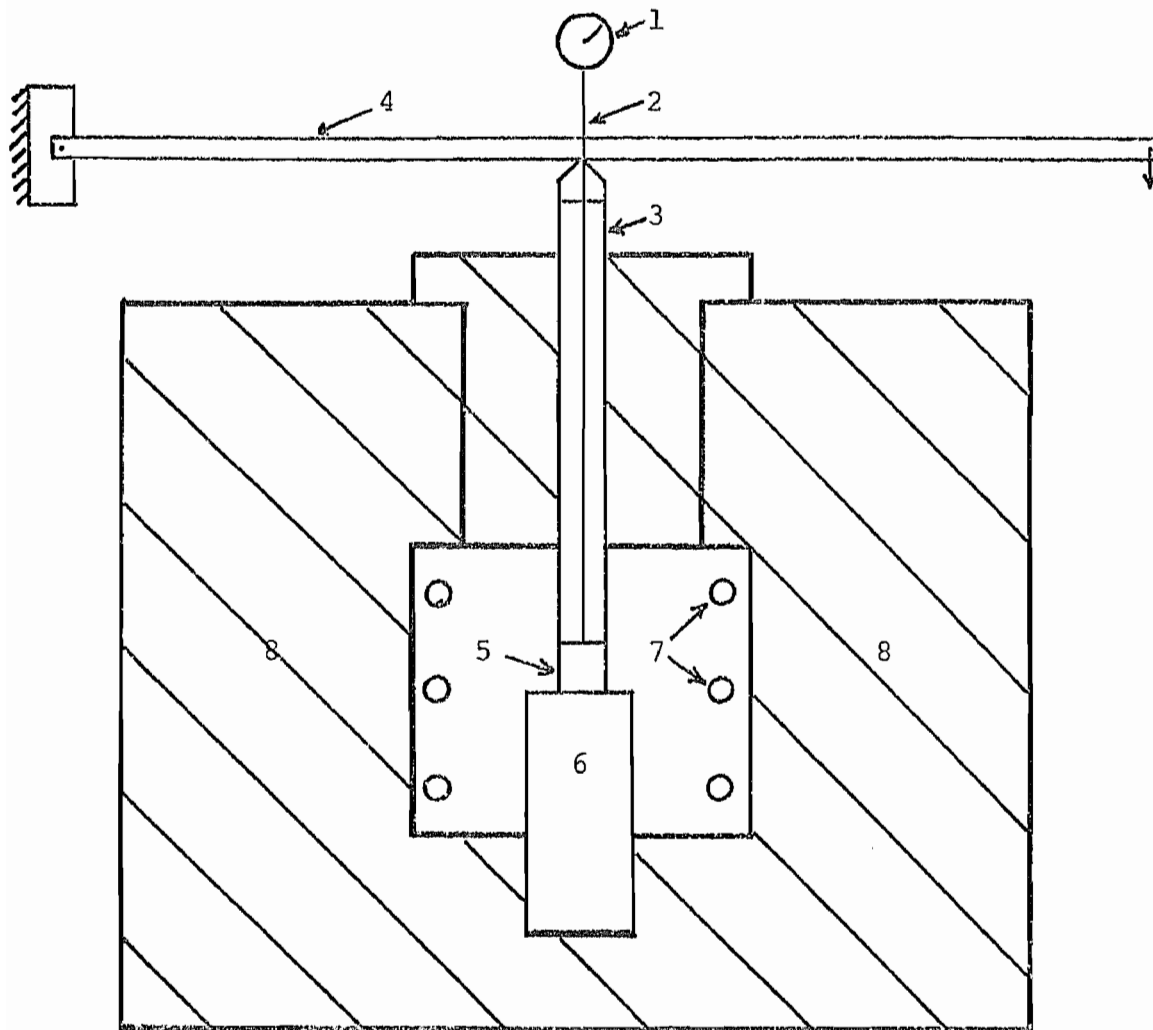
1. Dial gauge
2. Sapphire rod
3. Silicon carbide pushrod
4. Lever loading system
5. Sample
6. Silicon carbide base
7. Silicon carbide heating elements
8. Insulation (cross hatched)

Figure 3. Cross Section of Creep Furnace

stress at fracture is given by:

$$S = 2P/\pi DL$$

where: S = tensile strength, psi

P = compressive load at fracture, lbs.

D = sample diameter, inches

L = sample length, inches

D.   Phase Studies

The crystalline phases in the starting materials and fired samples were identified by X-ray diffraction. X-ray diffraction was also used to determine the ratio of α-alumina to mullite in fired samples. A calibration curve was constructed showing the ratio of the intensities of the (104) reflection from α-alumina and the (121) reflection from mullite in known mullite-alumina mixtures. The ratio of the same reflections in fired samples was employed to find the corresponding mullite to alumina ratio from the calibration curve.

Further studies of the phase assemblage were performed using the metallographic microscope. Sections of the fired samples were mounted in Bakelite and polished according to the procedure given in Appendix B.

E.   Electron Probe Microanalysis

The distribution of Al^{3+}, Si^{4+} and Na^+ ions in the fired samples was examined using the electron probe

microanalyzer. Polished sections of the samples were vapor coated with carbon and examined using a 15 KV electron beam. A KAP analyzing crystal was employed for detection of the characteristic X-rays. The distribution of the ions was recorded by photographing an oscilloscope display of the X-rays emitted from the sample.

IV RESULTS

The creep data for the 90% alumina -10% silica samples
are given in Appendix C. Typical deformation vs. time
curves are also included in Appendix C. The linear steady
state portion of the creep curves was analyzed by a linear
least squares regression of deformation on time. The steady
state creep rates shown in Table IV are the slopes of the
regression curves for each sample at four different tempera-
tures. The activation energies shown in Table IV were
calculated from the steady state creep rates as described in
section III-B. Graphs of the natural logarithm of creep
rate vs. reciprocal absolute temperature for each sample
group, Figures 4 through 10, show the temperature dependence
of the steady state creep rate.

Measurements of the mineralogical composition, bulk
density, apparent porosity and tensile strength were also
made to supplement the creep measurements. The phase compo-
sition of each sample as-fired and after the creep tests is
given in Table V. The mullite contents given in Table V
are the observed mullite contents expressed as a percentage
of the ideal mullite content, which for a 90% alumina-10%
silica composition is 35 weight percent. A metallographic
microscope was also utilized for examining the phase compo-
sition and microstructure of as-fired samples. Photomicro-
graphs of polished sections of certain selected samples are
shown in Figures 1 through 3, Appendix D. All of the

TABLE IV

STEADY STATE CREEP RATES AND ACTIVATION ENERGY FOR 90% ALUMINA SAMPLES

Sample*	Firing Treatment 1530°C (hours)	Steady State Creep Rate† (%/min. x 10⁴)				Activation Energy (kcal/mole)
		1450°C	1480°C	1500°C	1515°C	
S(0.04)	7	0.93	2.01	2.37	3.40	113
F(0.5)	7	0.51	1.35**	1.45	2.99	154
S(0.04)	3	2.40	4.04	5.00**	6.39	94
F(0.5)	3	1.03	1.29, 1.31	2.63**	6.11	143
S(0.3)	3	1.12**	2.47	3.30, 2.82	6.41	145
F(0.07)	3	1.17**	2.25	4.81, 3.89	5.85	156
S(0.5)	3	1.08	1.31	2.08	2.27**	75

* Numbers in parentheses indicate nominal sodium oxide content.

† Creep rates were measured at 100 psi compressive stress.

** Values obtained from appropriate regression curve, Figures 4-10.
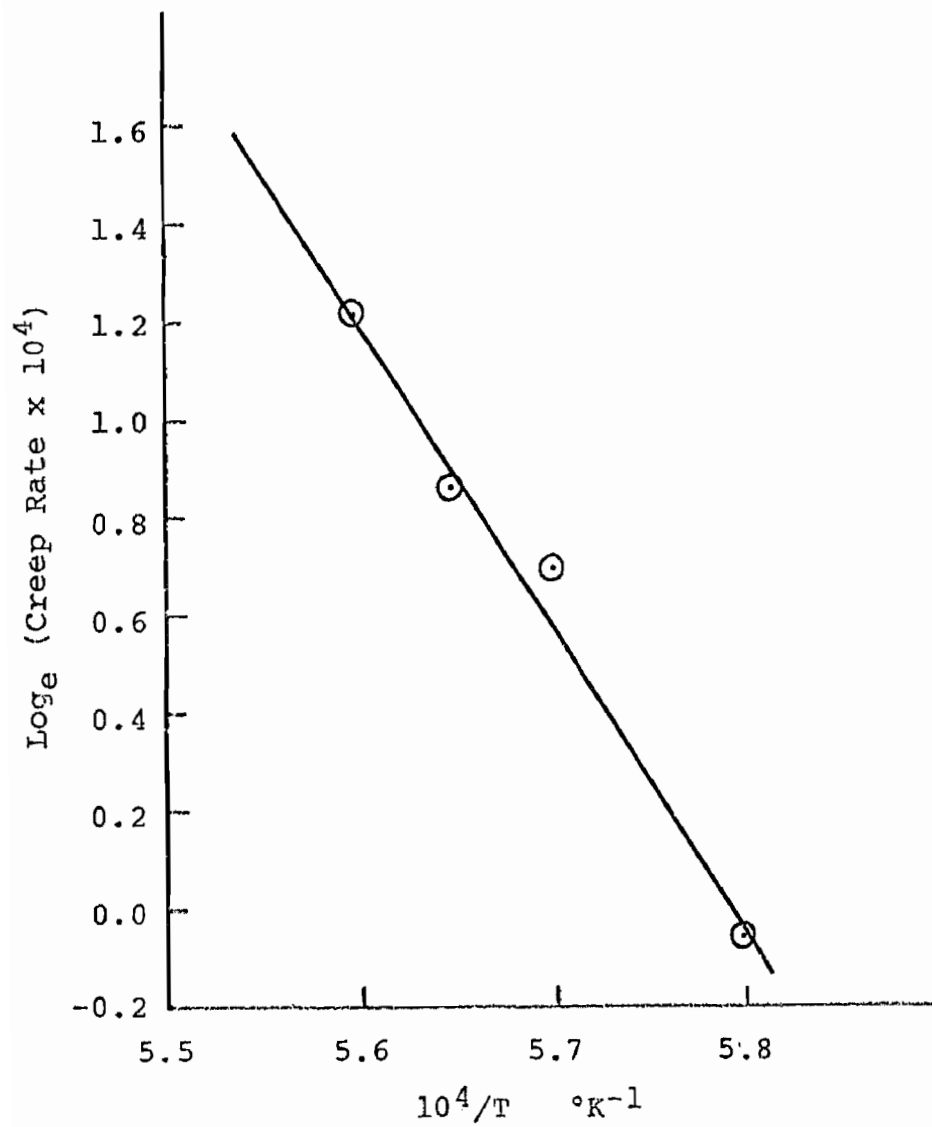
Figure 4. Temperature Dependence of Steady
State Creep Rate for S(0.04) Samples
Fired Seven Hours at 1530°C
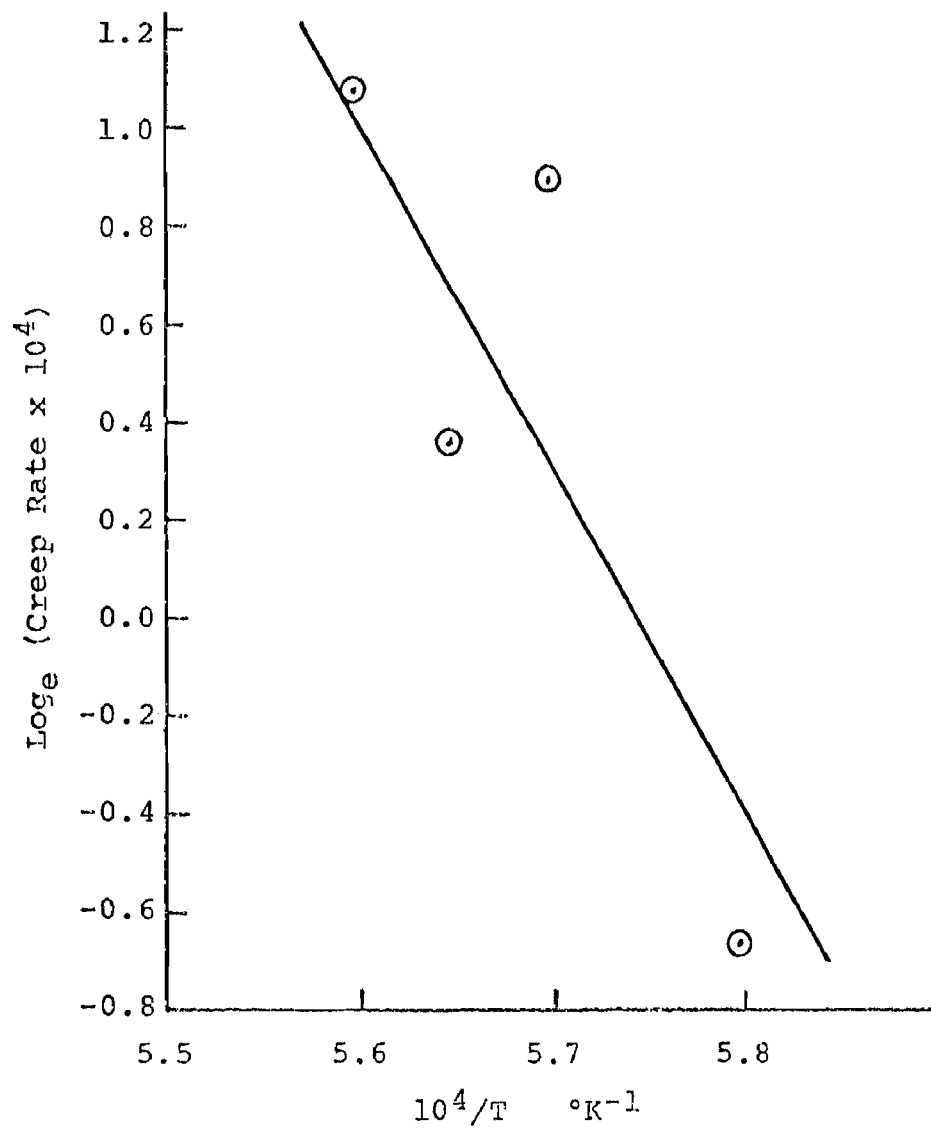
Figure 5.   Temperature Dependence of Steady
State Creep Rate for F(0.5) Samples
Fired Seven Hours at 1530°C
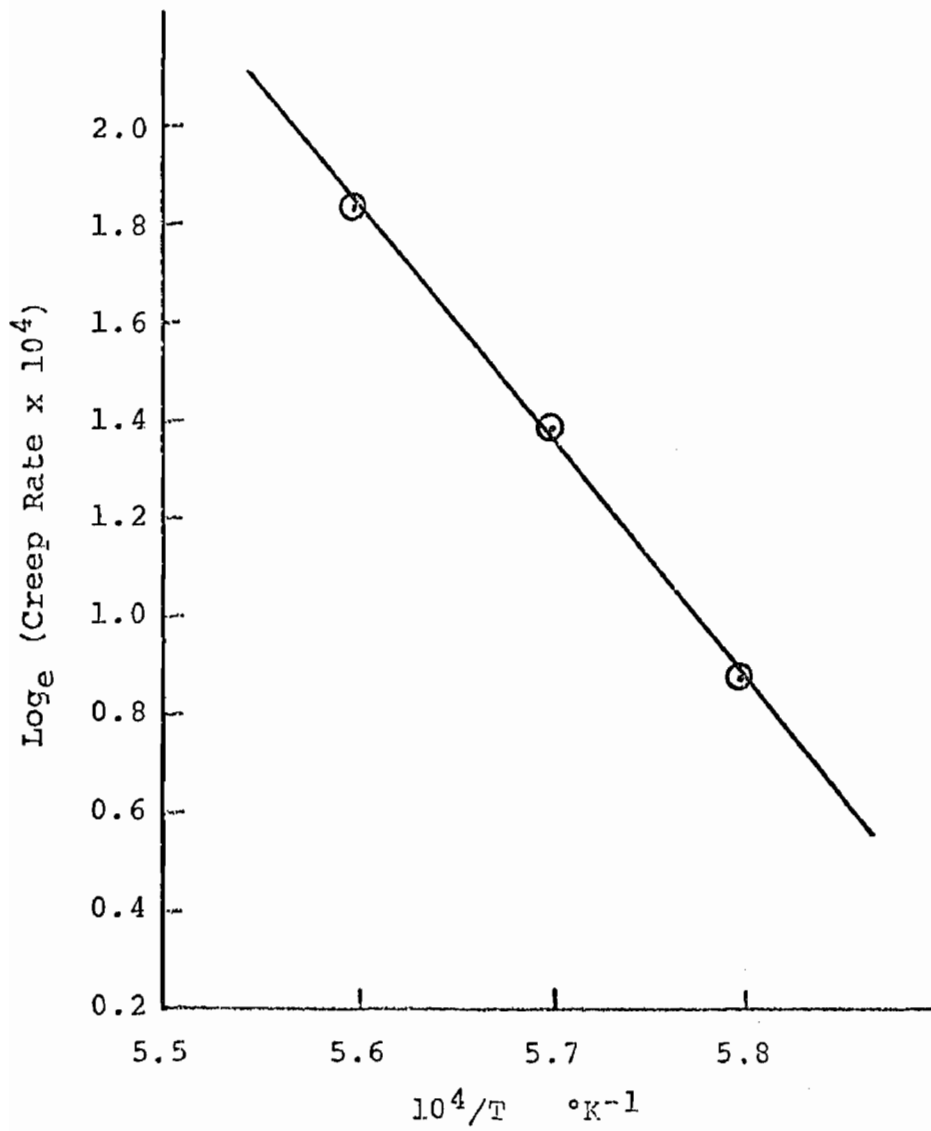
Figure 6. Temperature Dependence of Steady
State Creep Rate for S(0.04) Samples
Fired Three Hours at 1530°C
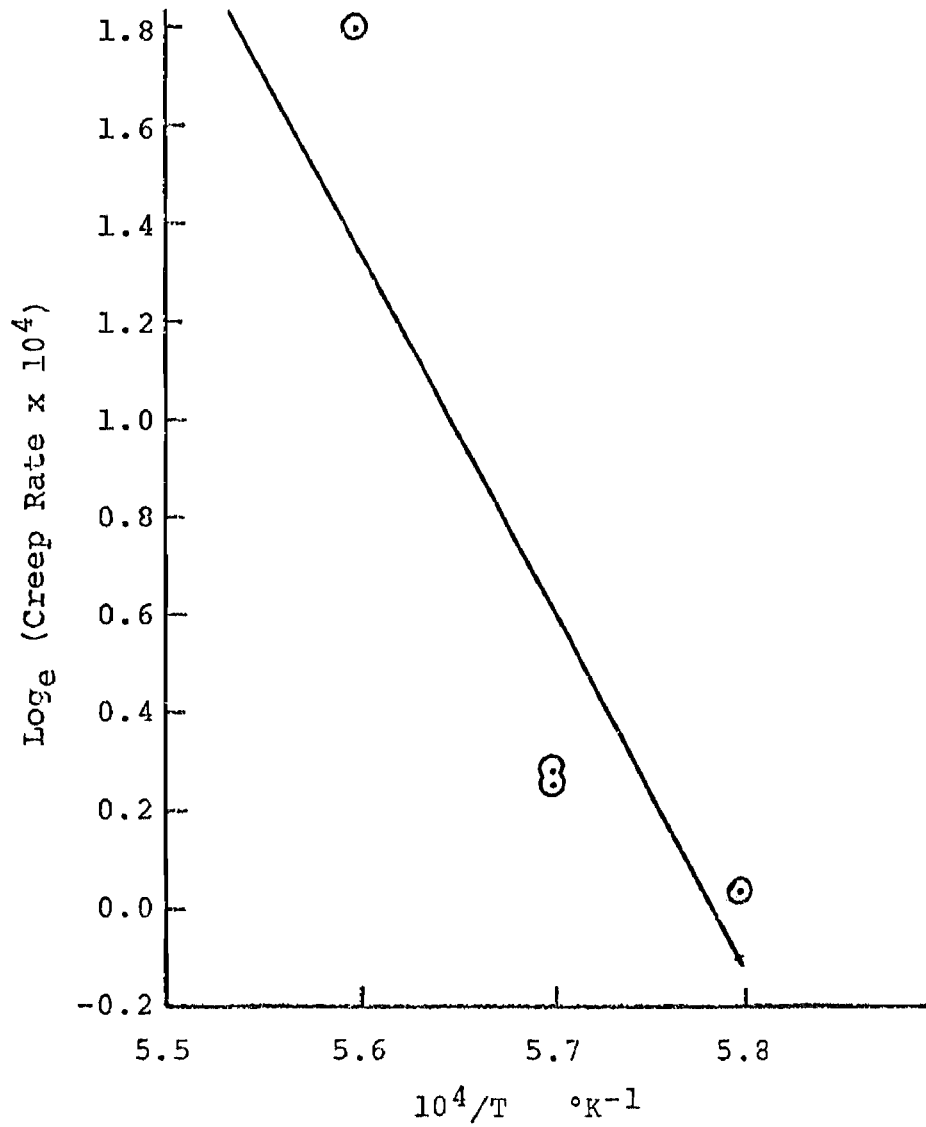
Figure 7. Temperature Dependence of Steady
State Creep Rate for F(0.5) Samples
Fired Three Hours at 1530°C
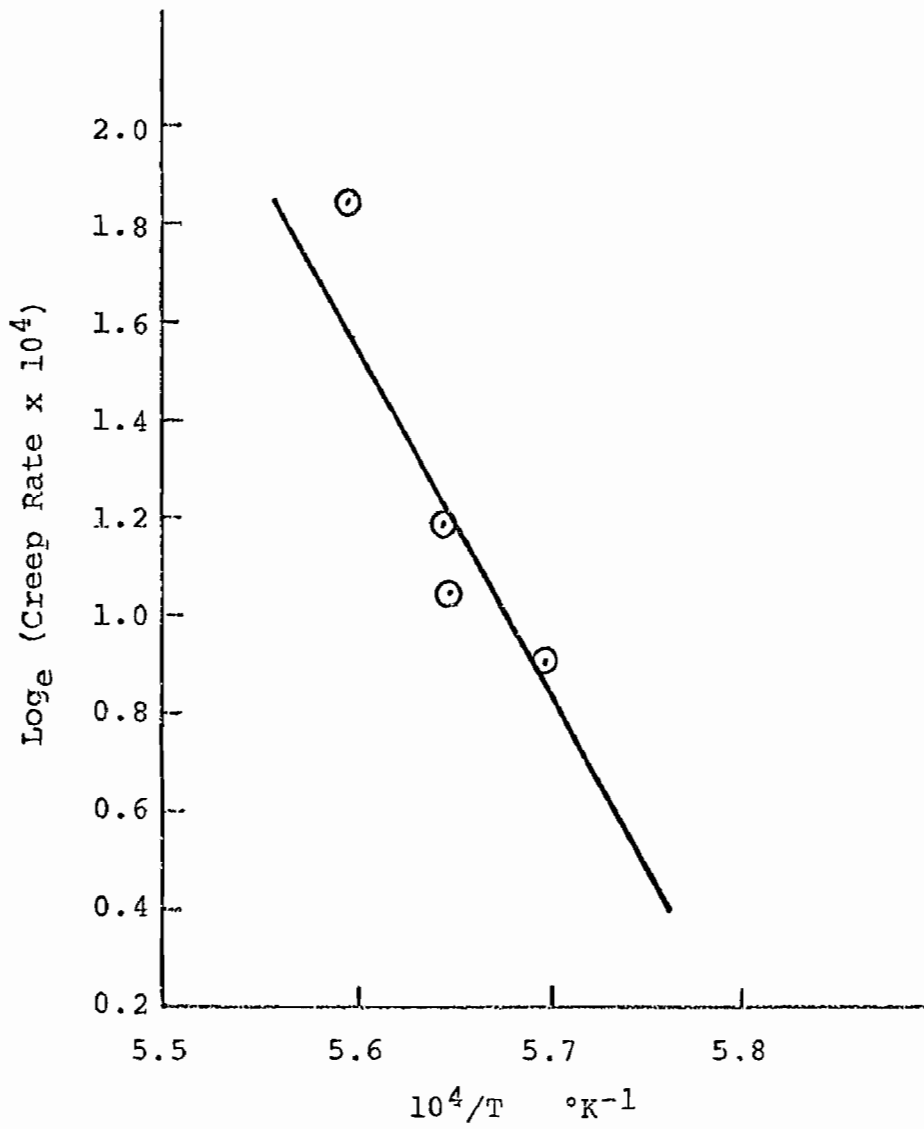
Figure 8. Temperature Dependence of Steady
State Creep Rate for S(0.3) Samples
Fired Three Hours at 1530°C
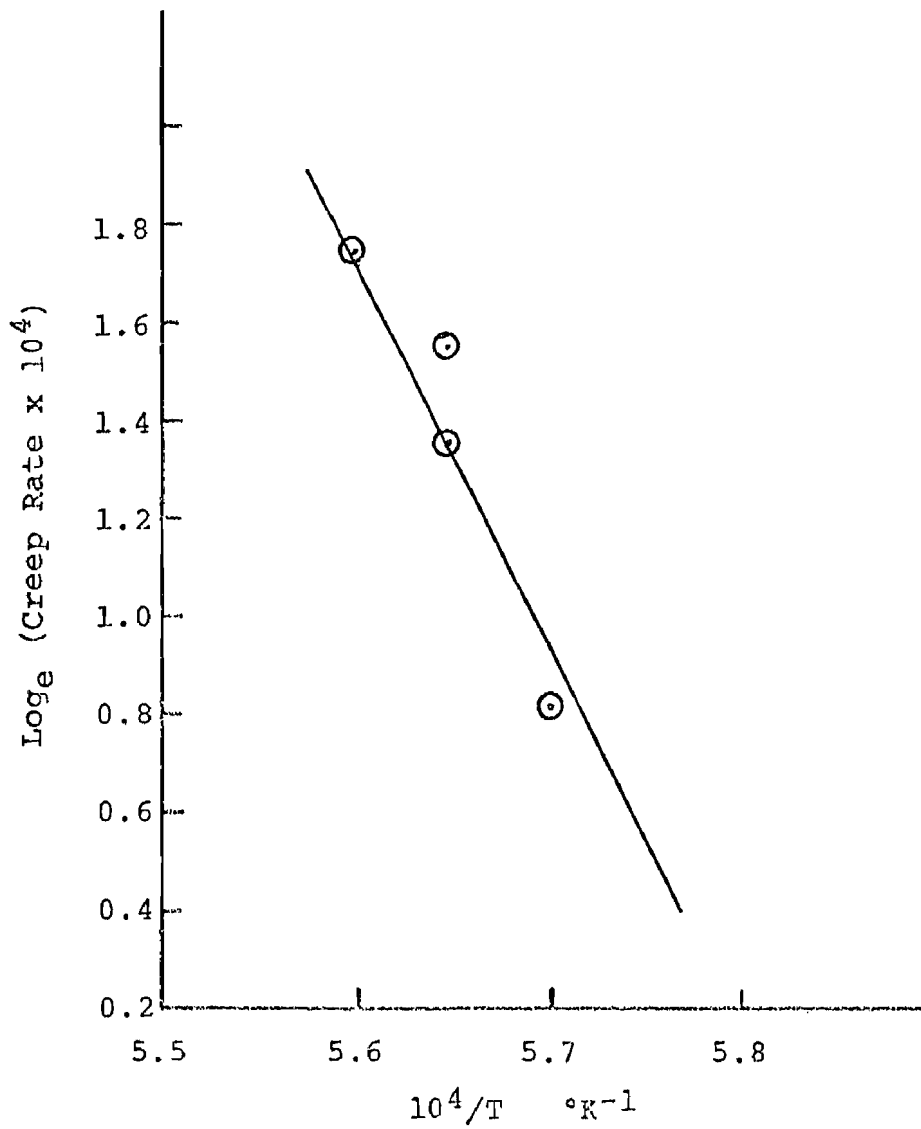
Figure 9. Temperature Dependence of Steady
State Creep Rate for F(0.07) Samples
Fired Three Hours at 1530°C
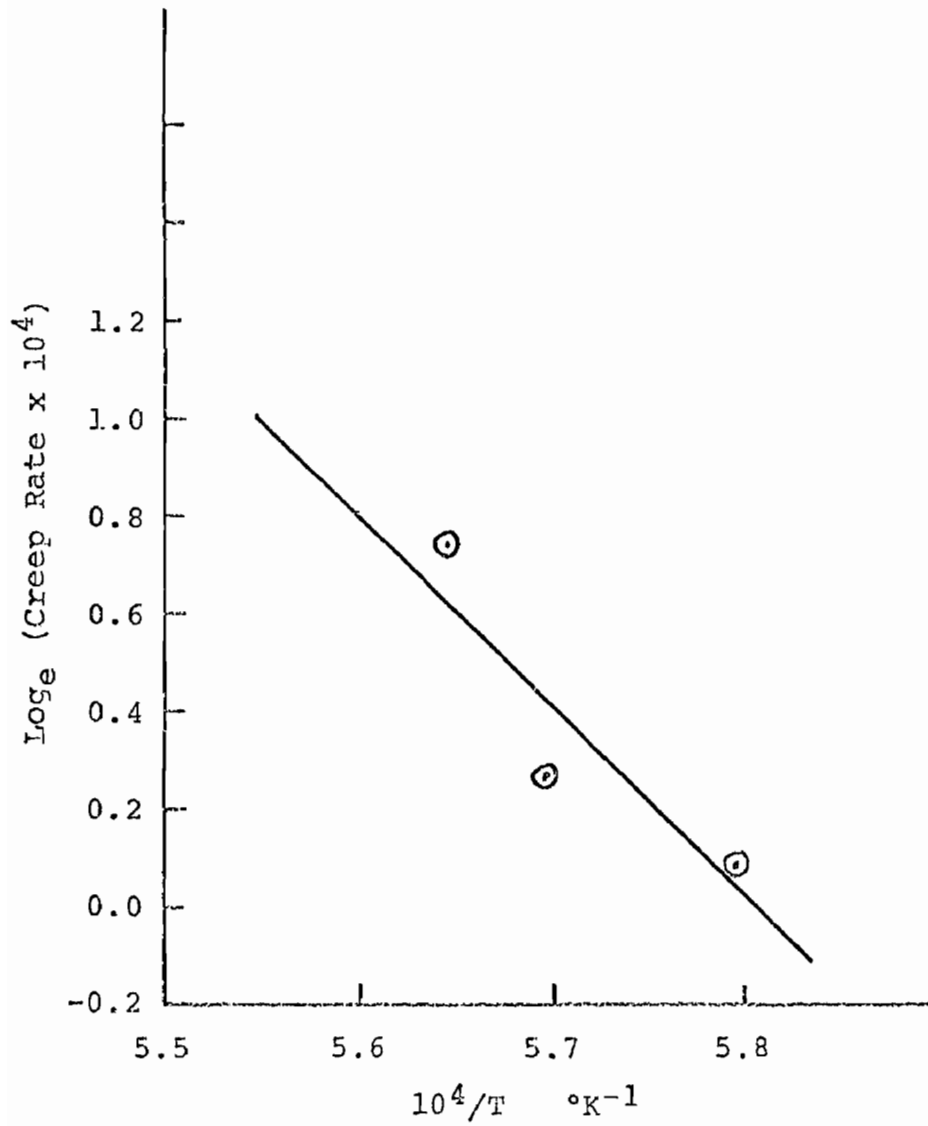
Figure 10.   Temperature Dependence of Steady
             State Creep Rate for Doped S(0.5)
             Samples Fired Three Hours at 1530°C

TABLE V

MINERALOGICAL COMPOSITION OF 90% ALUMINA SAMPLES AS DETERMINED BY X-RAY DIFFRACTION

Sample	Firing Treatment 1530°C (hours)	Crystalline Phases†	Mullite (% of theoretical)*				
			As-Fired	1450°C	1480°C	1500°C	1515°C
S(0.04)	7	α-alumina cristobalite mullite	17	--	25	36	29
F(0.5)	7	α-alumina mullite	42	--	55	49	57
S(0.04)	3	α-alumina cristobalite mullite	<9	22	--	--	17
F(0.5)	3	α-alumina mullite	31	53	51	--	51
S(0.3)	3	α-alumina mullite	43	--	53	52	54
F(0.07)	3	α-alumina mullite cristobalite	25	--	43	36	44
S(0.5)	3	α-alumina mullite	18	37	55	51	--

* Temperatures indicated are those of the creep tests.
† Pertains to samples as-fired and after creep tests.

physical properties given in Table VI were measured at room temperature.

TABLE VI

ROOM TEMPERATURE PROPERTIES OF 90% ALUMINA SAMPLES*

Sample	Firing Treatment 1530°C (hours)	Bulk Density (gm/cm³)	Apparent Porosity (percent)	Tensile Strength (psi)	Standard Deviation of Tensile Strength (psi)
S(0.04)	7	2.67	22.7	966	117
F(0.5)	7	2.84	21.7	1599	182
S(0.04)	3	2.64	25.6	406	50
F(0.5)	3	2.81	21.3	1442	108
S(0.3)	3	2.80	21.1	1180	196
F(0.07)	3	2.87	21.3	1116	115
S(0.5)	3	2.76	20.9	1704	142

* Property values represent averages of 20 samples.

V DISCUSSION OF RESULTS

A. General

It is not unusual for the deformation or creep charac-
teristics of polyphase ceramic materials to be the result
of several different mechanisms. In aluminosilicates, the
possible mechanisms include: (1) flow of a glassy phase,
(2) grain boundary sliding movement, and (3) plastic flow
within grains. Furthermore, it is conceivable for the
deformation to be the sum of two or more simultaneous
processes. Most investigators[6] agree that the creep of
ceramic materials including aluminosilicates, is strongly
influenced by the intergranular bonding matrix. Certain
types of intergranular phases are known to have a high
resistance to deformation at high temperature[8].

In the high alumina portion of the alumina-silica
system, refractories containing a well developed inter-
granular bonding matrix composed of mullite crystals show
relatively low creep rates. In contrast, aluminosilicates
containing glassy bonds usually exhibit higher creep rates[8,9]
under the same conditions. Thus, any physical or chemical
condition affecting the mineralogical composition of high
alumina refractories must be considered in interpreting
creep behavior. Those factors affecting the amount and
distribution of mullite and glassy phases are especially
important. In the present study, the mineralogical

composition of the 90% alumina samples and consequently the creep behavior was found to depend upon: (1) the heat treatment, (2) the amount and distribution of the sodium oxide present as an impurity, and (3) the reactivity of the alumina grain.

B. Significance of the Mineralogical Composition

In the 1450 to 1530°C temperature range employed in this work, the equilibrium phases of 90% alumina-10% silica compositions are mullite and α-alumina. X-ray diffraction clearly indicates, that equilibrium was not attained in any of the samples since the mullite contents listed in Table V are only about one-half of the theoretical mullite content. Silica which did not combine with alumina to form mullite remained as cristobalite or reacted with the sodium oxide and alumina to form a glassy phase.

1. Heat Treatment

The dependence of the creep rate upon the duration of heat treatment is illustrated by the S(0.04) and F(0.5) samples heated to 1530°C for three and seven hours, Table IV. Prolonged heating decreased the steady state creep rate and increased the activation energy for both the sintered and fused alumina samples. The primary difference in the mineralogical composition of the seven hour samples as compared to the three hour samples was an increase in mullite content, Table V. Thus, the decrease in creep rate

and increase in activation energy are consistent with the behavior expected for an increase in mullite content.

2. Sodium Oxide

A comparison of the creep rates given in Table IV, and shown graphically in Figures 11 and 12, for samples heated for three hours at 1530°C clearly show the effect of the sodium oxide impurity. Both sintered and fused alumina samples show decreased creep rates with increasing sodium oxide content.

The amount of sodium oxide impurity had a significant effect upon the mineralogical composition of both sintered and fused alumina samples. Evidence of its importance is illustrated by the higher mullite contents of the samples high in sodium oxide, Table V. Additionally the presence of cristobalite in low sodium oxide samples and its absence in high sodium oxide samples suggests that a small amount of glass is present in the latter samples since not all of the silica reacted to form mullite.

Evidence of the association of silica and sodium oxide in the high sodium oxide samples was obtained by electron probe microanalysis. Figure 6, Appendix D, shows the close association of sodium oxide and silica in the F(0.5) samples which is typical of high sodium oxide samples. This association of silica and sodium oxide is also evident in the doped S(0.5) samples, Figure 5, Appendix D. The sodium oxide in the S(0.04) samples on the other hand, is evenly
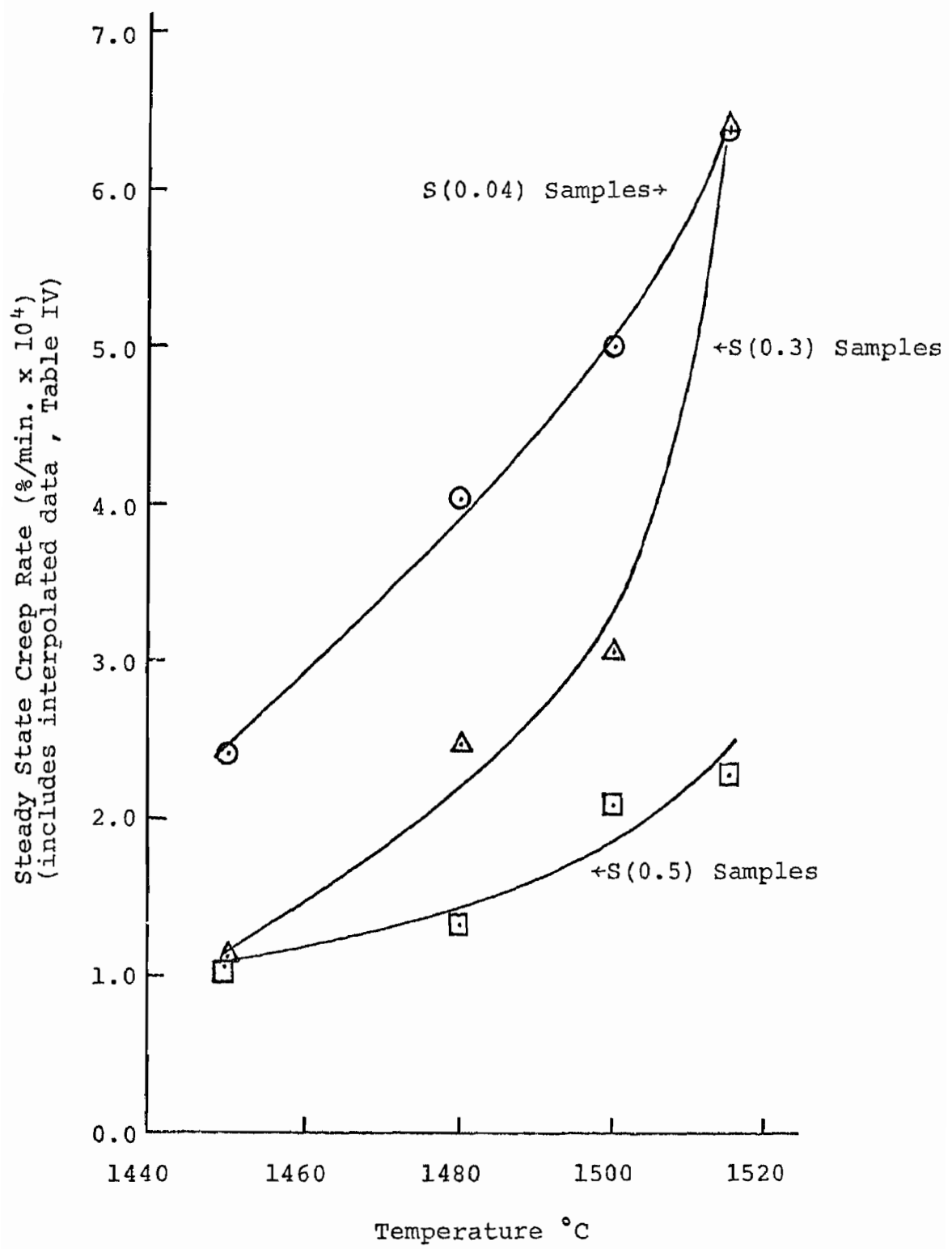
Figure 11. Effect of Temperature and Sodium Oxide on the Steady State Creep Rate of Sintered Alumina Samples Fired Three Hours at 1530°C.
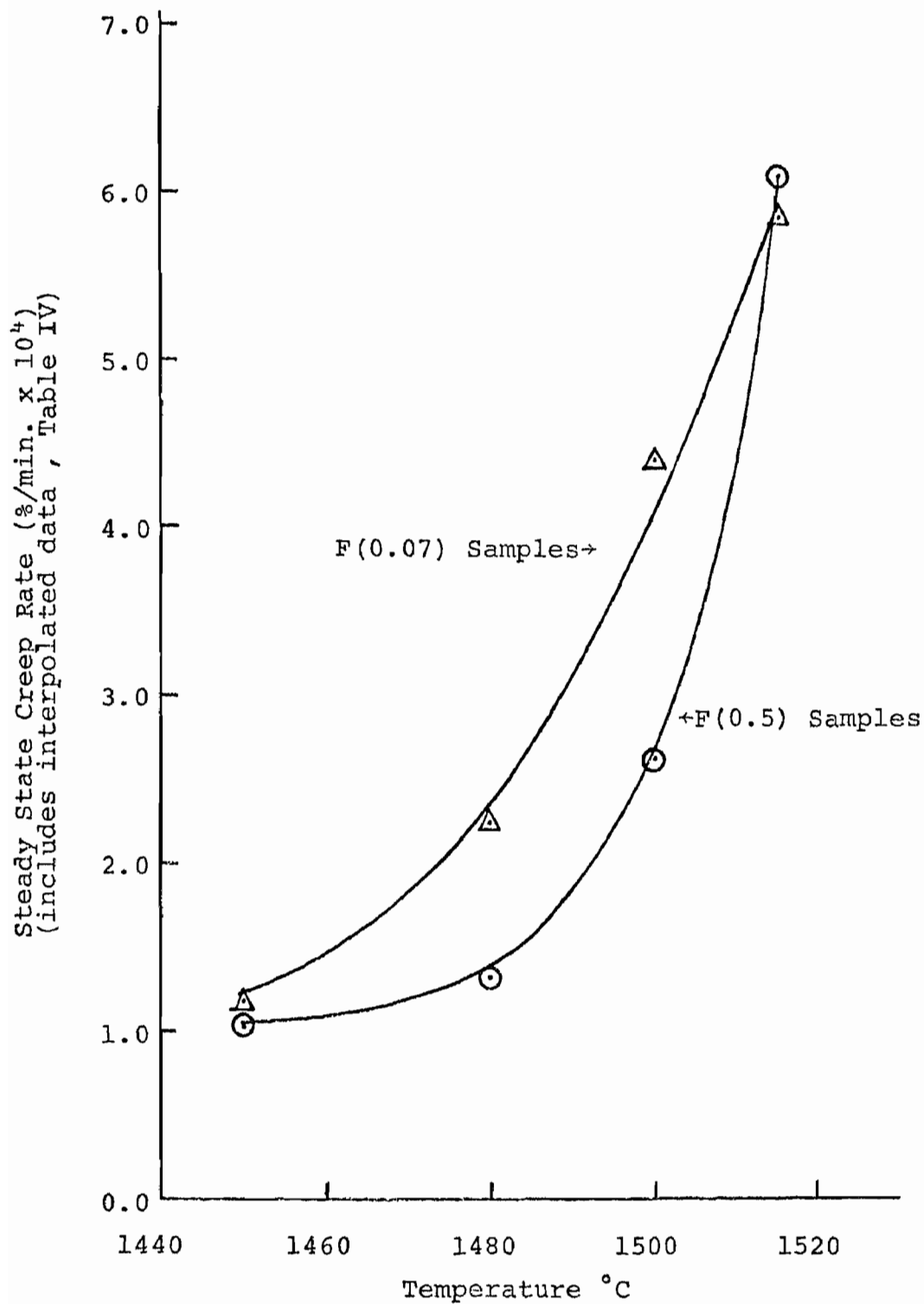
Figure 12. Effect of Temperature and Sodium Oxide
on the Steady State Creep Rate of
Fused Alumina Samples Fired Three Hours
at 1530°C.

distributed, Figure 4, Appendix D. These observations are considered to show that the silica uncombined in mullite, is combined with the sodium oxide in a glassy phase, especially in samples of high sodium oxide content. Furthermore, the presence of unreacted cristobalite in the S(0.04) and F(0.07) samples is indicative of the absence of the alkali flux.

The importance of sodium oxide in promoting intergranular bonding is illustrated further by the room temperature tensile strengths shown in Figure 13. The consistent increase in strength for samples of equivalent heat treatment, but higher sodium oxide contents,is indicative of better intergranular bonding. Since the intergranular bonding in these samples is composed of both mullite and glass in varying proportions, the tensile strengths do not show the separate contribution which these two phases make to the total intergranular bonding.

The effect of sodium oxide was most pronounced in the S(0.5) samples. The creep rates of these doped samples were lower than would be expected from their as-fired mullite content. Tentatively, this is attributed to two conditions: (1) the manner in which sodium oxide was introduced and (2) the change in mullite content during creep testing.

The introduction of sodium oxide as Na_2CO_3 provides a readily available flux for the silica in these samples. In contrast, the sodium oxide which is initially dissolved in the alumina grain in undoped samples is not expected to be
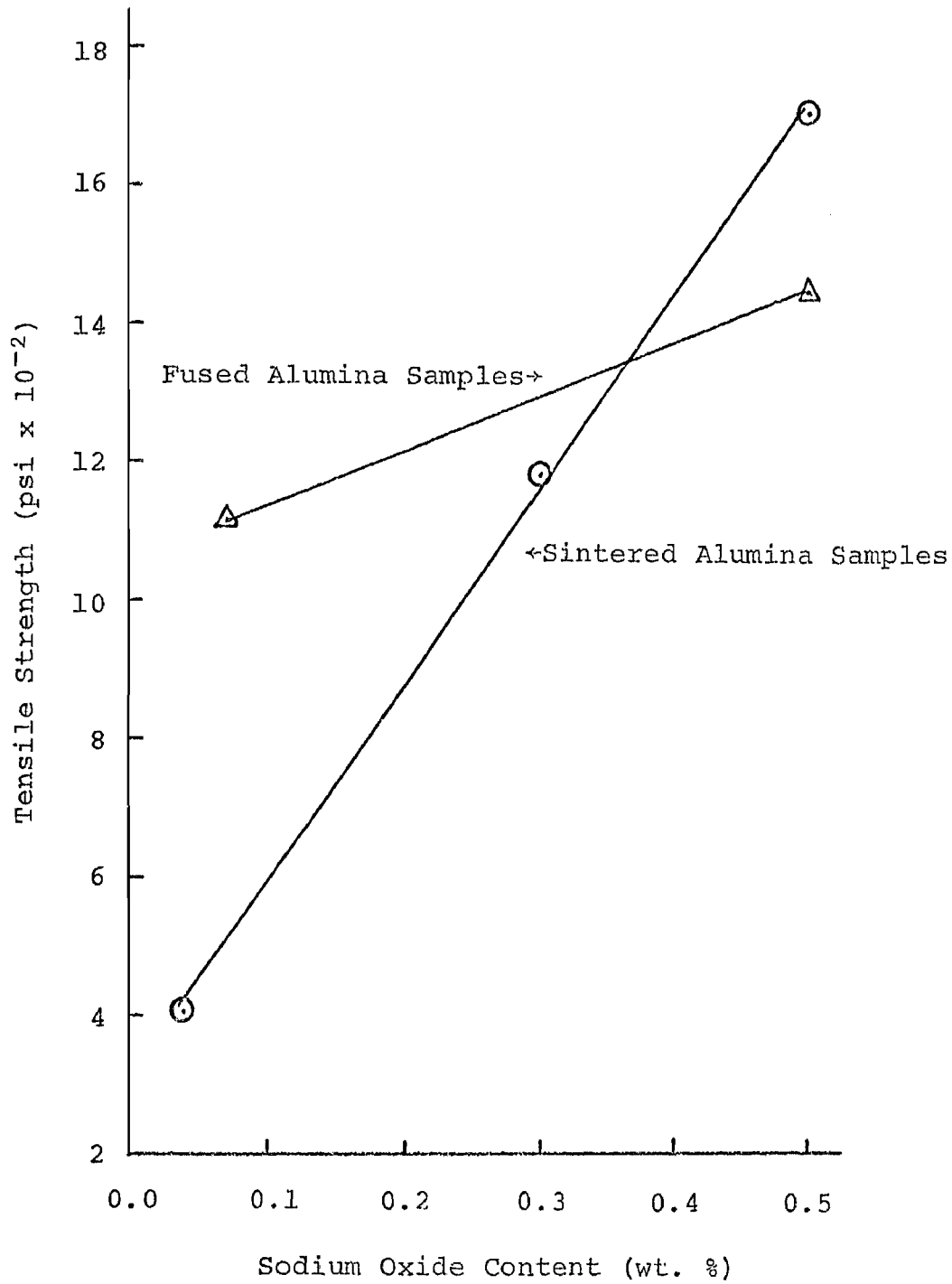
Figure 13.   Effect of Sodium Oxide on
Tensile Strength

as available for reaction with silica. The enhanced reactivity of the sodium oxide in doped S(0.5) samples is indicated by the relatively low as-fired mullite content, the absence of cristobalite, the low apparent porosity and the unusually high tensile strength. All of these properties suggest that the doped samples contain a greater amount of glassy phase than the undoped samples. The creep rates of the doped S(0.5) samples are lower than expected however, in view of the relative glass contents of these and other undoped samples. Generally an increase in glass content is expected to lead to higher creep rates.

A second explanation for the low creep rates of the doped S(0.5) samples is related to their mullite content. The mineralogical composition of these samples changed significantly during creep tests, as evidenced by the nearly three-fold increase in mullite content during the measurement at 1480°C (Table V). If this rapid formation of mullite is assumed to occur during the first few hours of the creep test, then the mullite content may have been substantially higher during the steady state portion of the measurement than that indicated by the as-fired condition. It should be noted that of all samples tested, the doped samples had the largest relative increase in mullite content.

3. Nature of the Alumina Grain

The differences observed in the creep behavior of samples containing sintered or fused alumina, but of

equivalent sodium oxide content and heat treatment are suggestive of differences in the reactivity of the two types of alumina. With the exception of the doped S(0.5) samples, the fused alumina samples always exhibited the lowest steady state creep rates for comparable conditions.

Samples S(0.04) and F(0.07) heat treated for three hours at 1530°C, Table IV, are good illustrations of this point. After firing at 1530°C the mullite content of the fused alumina sample was 25% of theoretical whereas that of the sintered alumina sample was only about 9% of theoretical. While the lower creep rates and higher activation energy for the fused alumina samples are consistent with their higher mullite content, this does not explain why mullite formed more rapidly in the fused alumina.

The reasons for the difference in the rate of mullite formation in the fused alumina samples as compared to essentially identical samples of sintered alumina are not completely known at this time. For the low sodium oxide samples the slightly higher sodium oxide content of the fused alumina (0.07%) as compared to the sintered alumina (0.04%) may be partially responsible. On the other hand, the mullite contents given in Table V for as-fired S(0.3) samples and F(0.5) samples show that mullite formation took place more rapidly in samples containing sintered alumina, 43% and 31% respectively. Nevertheless, the F(0.5) samples gave lower creep rates regardless of the lower mullite content.

Apparently, the difference in mullite contents of sintered and fused alumina cannot be entirely attributed to only the amount of the sodium oxide impurity. Some other factor or factors must influence the reactivity of the alumina grain. One plausible explanation for the apparent higher reactivity of the fused alumina grain of low sodium oxide content, is related to the different ways in which fused and sintered alumina are prepared. The freshly fractured surfaces of the monocrystalline fused alumina could conceivably be more reactive than the surface of the sintered grain.

The present work agrees with that of Clements and Vyse[8] who reported that the creep resistance of high alumina refractories containing fused grain was better than that of refractories containing sintered grain. With equivalent sodium oxide content and heat treatment, the lower creep rates observed for the fused alumina samples is now attributed to differences in the reactivity of the two types of alumina.

C. Temperature Dependence of the Creep Rate

The temperature dependence of the creep rates (i.e. activation energies) determined in this study was lower than expected. It was anticipated from the work of Pask and Hulse[6], that activation energies near 175 kcal/mole would be obtained for creep controlled by a mullite bonding matrix. Similarly, activation energies lower than 175 kcal/mole were

expected for samples of low mullite content, whereas activation energies higher than 175 kcal/mole were expected for samples undergoing phase changes during the creep tests. However, the activation energies calculated from the present data were lower than 175 kcal/mole even though phase changes were occurring during the creep measurements.

There is, however, a consistent correlation between the mullite content and the activation energy in samples of equivalent sodium oxide content, except for the doped S(0.5) samples. In the low sodium oxide samples F(0.07) and S(0.04), Table VII the higher activation energies are associated with the higher mullite contents irrespective of whether the increased mullite results from prolonged heat treatment or differences in the reactivity of the alumina grain. The activation energies for samples F(0.5) and S(0.04) heated for three and seven hours also show the effect of higher mullite content, Table VII.

The unexpectedly low activation energies observed for samples of reasonably high mullite content, S(0.3) and F(0.5) especially, are indicative of those for a glassy phase modified by the presence of mullite. With the exception of the doped S(0.5) samples, the S(0.04) and F(0.5) samples show an activation energy which increases with increasing mullite content. Since glass formation is considered most likely in the doped S(0.5) samples, a higher mullite content would be required to increase the activation energy comparable to that of the F(0.5) samples.

TABLE VII

MULLITE CONTENT AND ACTIVATION ENERGY FOR CREEP IN 90% ALUMINA SAMPLES

Activation Energy (kcal/mole)	Mullite Content* As-Fired	Mullite Content After* Creep Tests at 1515°C	Sample	Heat Treatment 1530°C (hours)
113	17	29	S(0.04)	7
154	42	57	F(0.5)	7
94	<9	17	S(0.04)	3
143	31	51	F(0.5)	3
145	43	54	S(0.3)	3
156	25	44	F(0.07)	3
75	18	~51	S(0.5)	3

* Percent of Theoretical

In samples of low sodium oxide content the activation energies also increase with increasing mullite content. These activation energies reflect a deformation process involving an intergranular bonding matrix consisting essentially of mullite and cristobalite with negligible glass content.

While the activation energies found in this study are lower than those determined previously by Pask and Hulse[6] for fireclay refractories the effects of mullite concentration are the same in both instances. That is, samples containing the most mullite exhibit the highest activation energies for creep.

VI SUMMARY AND CONCLUSIONS

The creep rates and activation energies were deter-
mined for 90% alumina refractories containing either
sintered or fused alumina and silica. These data were
correlated with the mineralogical composition. The miner-
alogical composition and hence the creep behavior, was found
to depend upon the heat treatment, the sodium oxide content
and the reactivity of the alumina grain.

It is concluded that:

1. Prolonged heat treatment gives the expected
results of increased mullite contents, lower
creep rates and higher activation energies.

2. Sodium oxide impurity in amounts up to 0.5%
accelerates mullite formation and also
enhances glass formation. Samples made from
sintered and fused alumina containing 0.3
and 0.5% Na_2O respectively, had lower creep

rates than comparable samples of sintered and
fused alumina containing 0.04 and 0.07% Na_2O,
respectively. The creep rates of the samples
of high sodium oxide content are consistent
with their higher mullite contents.

3. The differences observed in the creep rates and
activation energies for fused and sintered
alumina samples are attributed to differences
in the intergranular bonding matrix. The

availability of the sodium oxide for reaction

its distribution, and the amount present are all

considered important to the type of matrix

developed.

VII   SUGGESTIONS FOR FUTURE WORK

During this investigation several interesting results were obtained which could not be explored fully. Two of these observations, namely: (1) the difference in reactivity of fused and sintered alumina, and (2) the importance of sodium oxide in accelerating mullite and glass formation, are the bases for suggesting the following studies.

1. A study of the surfaces of sintered and fused alumina should be undertaken to fully characterize the surface properties and isolate differences between the two materials. Physical as well as chemical properties are of importance since both can influence the reactivity of the grain.

2. A systematic study of the effect of sodium oxide on the properties of high alumina refractories is warranted. Since sodium oxide in amounts up to 0.5 wt. % enhances both mullite and glass formation, it is conceivable that there is an optimum amount of sodium oxide which would promote maximum mullite formation while maintaining a relatively low amount of glass. The optimum may vary according to the nature of the alumina grain, the amount of silica present,

and also according to the desired properties
of the materials.

BIBLIOGRAPHY

1. R. E. Birch, "Refractories in Transition," Iron and Steel Engineer, October 1966.

2. A. J. Kennedy, Processes of Creep and Fatigue in Metals, pp 147-273, John Wiley and Sons Inc., New York (1963) 480 pp.

3. O. H. Wyatt, "Transient Creep in Pure Metals," Proc. Phys. Soc. London B66 495 (1953).

4. J. E. Dorn, "The Spectrum of Activation Energies for Creep," Creep and Recovery pp 255-83, ASM Cleveland, Ohio (1957) 372 pp.

5. P. Gibbs and H. Eyring, "A Theory for Creep of Ceramic Bodies Under Constant Load," Can. J. Res. 27B (4) 374-86 (1949).

6. C. O. Hulse and J. A. Pask, "Analysis of Deformation of a Fireclay Refractory," J. Am. Ceram. Soc. 49 (6) 312-18 (1966).

7. W. Kauzmann, "Flow of Solid Metals from the Standpoint of Chemical-Rate Theory," Trans. AIME 143 57-83 (1941).

8. J. F. Clements and J. Vyse, "Creep Measurements on Some High-Alumina Refractories," Trans. Brit. Ceram. Soc. 65 (2) 59-85 (1966).

9. B. A. Weichula and A. L. Roberts, "Elastic and Viscous Properties of Alumino-Silicate Refractories," Trans. Brit. Ceram. Soc. 51 (3) 173-97 (1952).

10. U. U. Chi and R. B. Sosman, "Deformation of a Kaolinite Body Under Stress at High Temperatures," Am. Ceram. Soc. Bull. 40 (7) 426-31 (1961).

APPENDIX

APPENDIX A

RATE PROCESS THEORY OF CREEP

The flow units considered responsible for creep deformation are assumed to be density fluctuations which are present in a material at high temperature. These fluctuations can persist for long periods because of the surrounding potential barriers[5]. The fraction of flow units which are thermally activated is given by the Boltzman distribution law as follows:

$$N/No = \exp(-F/RT) \tag{1}$$

where: N = number of activated units

No = total number of units

F = activation energy (potential barrier)

R = gas constant

T = absolute temperature

When an external stress is applied the stress modified barriers are designated by $F+\Delta F$ and $F-\Delta F$. For a given temperature the number of activated units proceeding in the forward and reverse directions are proportional to $\exp(-F+\Delta F)/RT$ and $\exp(F-\Delta F)/RT$ respectively[2]. The net flux in the forward direction i.e. the direction to relieve stress is then:

$$dn/dt = A \cdot \exp(-F/RT)[\exp\Delta F/RT) - \exp(-\Delta F/RT)] \tag{2}$$

$$\text{or } dn/dt = 2A \cdot \exp(-F/RT) \cdot \text{Sinh}(\Delta F/RT) \tag{3}$$

where: n = number of flow units

t = time

A = constant

F = barrier height (activation energy)

R = gas constant

T = absolute temperature

The constant A is dependent upon temperature, stress and structure. However the exponential term is the most important temperature term. According to Gibbs and Eyring[5]:

$$A = K\kappa T/h \tag{4}$$

where: K = transmission coefficient

κ = Boltzman's constant

T = absolute temperature

h = Plank's constant

The factor $\kappa T/h$ is termed the universal frequency factor and determines the rate of passage of the fluctuations over their respective barriers. The transmission coefficient, K, expresses the ratio of the number of fluctuations passing their barriers to the number having sufficient energy to surmount their barriers.

The change in barrier height, ΔF, as a function of stress is:

$$\Delta F = b\sigma \tag{5}$$

where: b = constant (volume dimensions)

σ = stress

Upon substituting values of ΔF and A from equations 4 and 5 into equation 3, the expression for the rate of passage of fluctuations over their barriers becomes:

$$dn/dt = 2 K \cdot (\kappa T/h) \exp(-F/RT) \cdot \text{Sinh}(b\sigma/RT) \qquad (6)$$

To convert this rate to creep rate, the following relation-ship is used:

$$S = (\delta/L)(dn/dt) \qquad (7)$$

where: S = creep rate

δ = component of creep in the stress direction for one jump

L = distance between flow units

The expression for creep rate as a function of stress and temperature becomes:

$$S = (\delta/L)(dn/dt) = (2K\delta/L)(\kappa T/h) \exp(-F/RT) \cdot \text{Sinh}(b\sigma/RT) \qquad (8)$$

APPENDIX B

POLISHING PROCEDURE FOR ALUMINA SAMPLES

1. Silicon carbide abrasive papers of the successive sizes 120, 320, 400, and 600 grit were used for rough polishing. The samples were held on each size for about 5 minutes with water being added to the lap as a coolant.

2. The intermediate polishing was done using diamond grit in the successive sizes 16, 6, 1, and $\frac{1}{4}$ micron. The paste containing the diamond abrasive was smeared onto a hardcloth for the three largest sizes and onto silk for the $\frac{1}{4}$ micron size.

3. The final polishing consisted of a 4 hour treatment in a Vibra-met polisher using 0.05 micron alumina in a water suspension.

APPENDIX C

TABLE C-I

CREEP DATA 1515°C, 100 psi, 7 HOUR SAMPLES

Deformation (%)

Time (Min.)	S(0.04) Sample	F(0.5) Sample
1	0.115	0.000
3	0.146	0.000
15	0.230	0.000
30	0.284	0.000
100	0.405	0.100
653	0.775	0.390
693	0.796	0.422
723	0.819	0.424
760	0.819	0.424
798	0.827	0.433
835	0.848	0.433
900	0.880	0.454
935	0.893	0.489
990	0.893	0.510
1055	0.924	0.520
1105	0.935	0.543
1145	0.955	0.564
1205	0.976	0.585
1255	1.001	0.589
1305	1.020	0.598
1370	1.036	0.615
1410	1.049	0.617
1480	1.059	0.639
1530	1.080	0.659
1590	1.091	0.660

TABLE C-II

CREEP DATA 1500°C, 100 psi, 7 HOUR SAMPLES

Deformation (%)

Time (Min.)	S(0.04) Sample	F(0.5) Sample
1	0.042	0.023
4	0.1o0	0.044
33	0.265	0.092
72	0.342	0.111
98	0.388	0.129
642	0.787	0.280
690	0.798	0.291
728	0.834	0.308
784	0.838	0.313
855	0.854	0.320
897	0.880	0.326
944	0.873	0.329
985	0.881	0.316
1072	0.909	0.346
1143	0.913	0.350
1236	0.939	0.368
1334	0.964	0.384
1389	0.971	0.392
1442	0.985	0.396
1474	1.001	0.413
1511	1.015	0.418
1560	1.015	0.418

TABLE C-III

CREEP DATA 1480°C, 100 psi, 7 HOUR SAMPLES

Deformation (%)

Time (Min.)	S(0.04) Sample	F(0.5) Sample
1	0.054	0.055
3	0.088	0.111
6	0.099	0.145
30	0.177	0.212
65	0.203	0.261
90	0.232	0.278
160	0.276	0.312
220	0.304	0.341
340	0.362	0.421
500	0.425	0.496
580	0.452	0.545
620	0.467	0.560
685	0.453	0.579
730	0.468	0.583
800	0.472	0.598
1300	0.581	0.731
1360	0.605	0.755
1391	0.605	0.766
1430	0.620	0.770
1472	0.633	0.783
1615	0.664	0.837
1700	0.674	0.835
1790	0.681	0.842
1825	0.692	0.854
1935	0.705	0.889
2015	0.725	0.898
2055	0.725	0.898
2105	0.736	0.909
2155	0.733	0.929

TABLE C-IV

CREEP DATA 1450°C, 100 psi, 7 HOUR SAMPLES

	Deformation (%)	
Time (Min.)	S(0.04) Sample	F(0.5) Sample
1	0.000	0.000
5	0.012	0.018
10	0.021	0.026
25	0.026	0.038
50	0.026	0.038
75	0.036	0.047
100	0.036	0.056
140	0.047	0.074
200	0.047	0.083
260	0.054	0.097
350	0.072	0.111
400	0.072	0.111
450	0.076	0.106
545	0.076	0.106
610	0.087	0.115
660	0.100	0.125
735	0.096	0.131
810	0.100	0.143
1395	0.180	0.156
1445	0.175	0.177
1515	0.177	0.170
1565	0.179	0.181
1655	0.179	0.181
1695	0.190	0.181
1745	0.201	0.189
1810	0.196	0.195
1875	0.210	0.197
1990	0.208	0.186
2105	0.227	0.184
2190	0.231	0.188

TABLE C-V

CREEP DATA 1450°C, 100 psi, 3 HOUR SAMPLES

Deformation (%)

Time (Min.)	S(0.04) Sample	F(0.5) Sample
1	0.040	0.009
3	0.080	0.028
5	0.109	0.036
10	0.129	0.056
44	0.198	0.105
80	0.239	0.135
130	0.287	0.163
170	0.321	0.187
184	0.323	0.189
250	0.365	0.189
326	0.411	0.204
1037	0.625	0.314
1114	0.646	0.314
1280	0.684	0.332

TABLE C-VI

CREEP DATA, 1480°C, 100 psi, 3 HOUR SAMPLES

Deformation (%)

Time (Min.)	S(0.04) Sample	F(0.5) Sample
60	0.049	0.018
90	0.062	0.020
130	0.082	0.041
235	0.119	0.047
317	0.175	0.072
405	0.205	0.080
475	0.215	0.080
540	0.246	0.080
607	0.267	0.090

TABLE C-VII

CREEP DATA 1515°C, 100 psi, 3 HOUR SAMPLES

	Deformation (%)	
Time (Min.)	S(0.04) Sample	F(0.5) Sample
2	0.101	0.039
4	0.144	0.051
13	0.144	0.062
30	0.221	0.087
600	0.109	0.753
644	1.123	0.794
692	1.154	0.824
733	1.174	0.844
770	1.225	0.874
825	1.247	0.916
883	1.304	0.952
933	1.325	1.002
980	1.366	1.022
1025	1.380	1.047
1067	1.401	1.067
1140	1.442	1.118
1253	1.572	1.125
1323	1.548	1.222
1393	1.571	1.244
1444	1.593	1.256
1480	1.605	1.278
1529	1.617	1.290

TABLE C-VIII

CREEP DATA, 1450°C, 100 psi, 3 HOUR SAMPLES

Deformation (%)

Time (Min.)	S(0.5) Doped Sample	F(0.5) Sample
1	0.025	0.010
3	0.043	0.030
10	0.062	0.052
40	0.075	0.062
130	0.092	0.139
180	0.128	0.197
240	0.186	0.283
280	0.141	0.280
305	0.133	0.280
345	0.118	0.258
445	0.110	0.248
520	0.143	0.276
587	0.145	0.299
655	0.139	0.303
703	0.165	0.319
1270	0.226	0.400
1332	0.227	0.401
1390	0.225	0.409
1440	0.248	0.422
1537	0.250	0.403
1610	0.268	0.379
1667	0.280	0.423
1730	0.287	0.419
1773	0.298	0.461
1828	0.279	0.432
1962	0.288	0.441
2018	0.271	0.435
2086	0.303	0.435

TABLE C-IX

CREEP DATA 1480°C, 100 psi, 3 HOUR SAMPLES

Deformation (%)

Time (Min.)	F(0.5) Sample	S(0.5) Sample
1	0.060	0.031
3	0.080	0.062
7	0.099	0.083
15	0.118	0.104
25	0.118	0.114
609	0.300	0.150
660	0.309	0.181
727	0.312	0.195
788	0.308	0.158
849	0.324	0.185
913	0.348	0.190
963	0.391	0.195
1040	0.388	0.202
1100	0.346	0.157
1146	0.382	0.195
1245	0.395	0.261
1285	0.419	0.265
1330	0.413	0.280
1380	0.402	0.268
1430	0.412	0.238
1495	0.412	0.299
1525	0.404	0.291
1580	0.415	0.241

TABLE C-X

CREEP DATA 1500°C, 100 psi, 3 HOUR SAMPLES

Deformation (%)

Time (Min.)	S(0.5) Doped Sample	F(0.07) Sample
1	0.129	0.139
3	0.140	0.208
5	0.172	0.244
10	0.183	0.324
25	0.290	0.440
40	0.344	0.638
582	0.764	1.392
642	0.764	1.415
704	0.811	1.512
758	0.819	1.510
872	0.864	1.558
928	0.896	1.593
993	0.900	1.599
1053	0.926	1.609
1116	0.932	1.636
1195	0.905	1.701
1285	0.943	1.706
1350	0.947	1.735
1410	0.947	1.740
1470	0.947	1.740

TABLE C-XI

CREEP DATA 1515°C, 100 psi, 3 HOUR SAMPLES

Deformation (%)

Time (Min.)	F(0.07) Sample	S(0.3) Sample
1	0.109	0.080
3	0.229	0.216
10	0.382	0.387
30	0.589	0.603
573	1.975	2.063
626	2.044	2.112
678	2.084	2.142
750	2.122	2.194
800	2.160	2.244
850	2.232	2.297
867	2.234	2.311
920	2.266	2.343
973	2.285	2.353
1090	2.345	2.426
1180	2.402	2.509
1246	2.403	2.521
1310	2.447	2.567
1363	2.478	2.588
1436	2.509	2.609

TABLE C-XII

CREEP DATA 1480°C, 100 psi, 3 HOUR SAMPLES

	Deformation (%)	
Time (Min.)	S(0.3) Sample	F(0.07) Sample
1	0.062	0.031
3	0.083	0.052
5	0.093	0.062
15	0.124	0.082
28	0.176	0.134
576	0.496	0.594
619	0.496	0.594
666	0.514	0.594
712	0.526	0.586
756	0.546	0.586
800	0.567	0.627
862	0.616	0.675
918	0.607	0.667
968	0.615	0.695
1050	0646	0.716
1104	0.646	0.716
1214	0.675	0.714
1305	0.677	0.757
1350	0.690	0.739
1446	0.721	0.749

TABLE C-XIII

CREEP DATA 1500°C, 100 psi, 3 HOUR SAMPLES

Deformation (%)

Time (Min.)	F(0.07) Sample	S(0.3) Sample
1	0.022	0.273
3	0.022	0.352
5	0.056	0.412
15	0.124	0.534
30	0.202	0.660
60	0.236	0.785
685	1.037	1.642
720	1.084	1.667
780	1.079	1.673
840	1.133	1.693
900	1.186	1.725
965	1.231	1.737
1040	1.349	1.845
1085	1.354	1.839
1135	1.348	1.833
1200	1.347	1.831
1260	1.365	1.838
1335	1.401	1.875
1380	1.400	1.862
1430	1.424	1.887
1494	1.437	1.923
1550	1.455	1.941
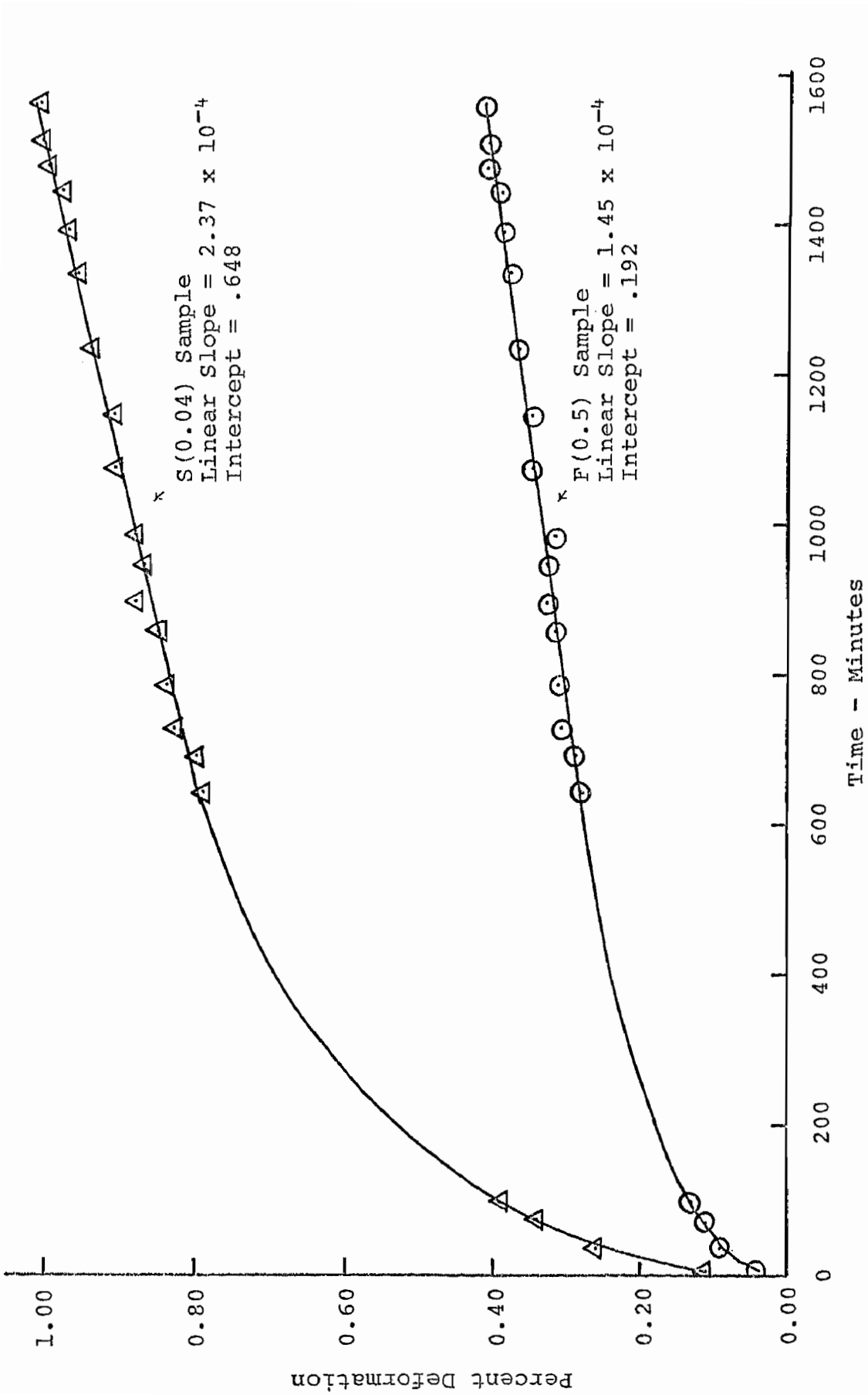
Figure C-1. Creep Curve Showing Typical Data Obtained at 1500°C. (See Table C-II)

S(0.04) Sample
Linear Slope = 2.37 x 10^{-4}
Intercept = .648

F(0.5) Sample
Linear Slope = 1.45 x 10^{-4}
Intercept = .192

APPENDIX D

PHOTOMICROGRAPHS AND ELECTRON PROBE MICROANALYSIS

Figures 1-3 are photomicrographs of polished sections
of fired samples. In these figures, alumina grains are
represented by the large light colored irregular shapes
while mullite grains appear as the smaller more angular or
elongated grains and as the light colored regions adjacent
to the alumina grains. Some mullite grains connecting
alumina grains are evident.

Figures 4-6 are photographs of an oscilloscope display
of the back scattered electrons and X-rays emitted from the
samples under an electron beam. The four scans in each
figure cover the same area of the sample, thus the distri-
bution of ions in that area is represented by the intensity
of characteristic X-rays emitted. The relative intensity
of the emitted radiation is represented by the density of
white dots in the photographs.
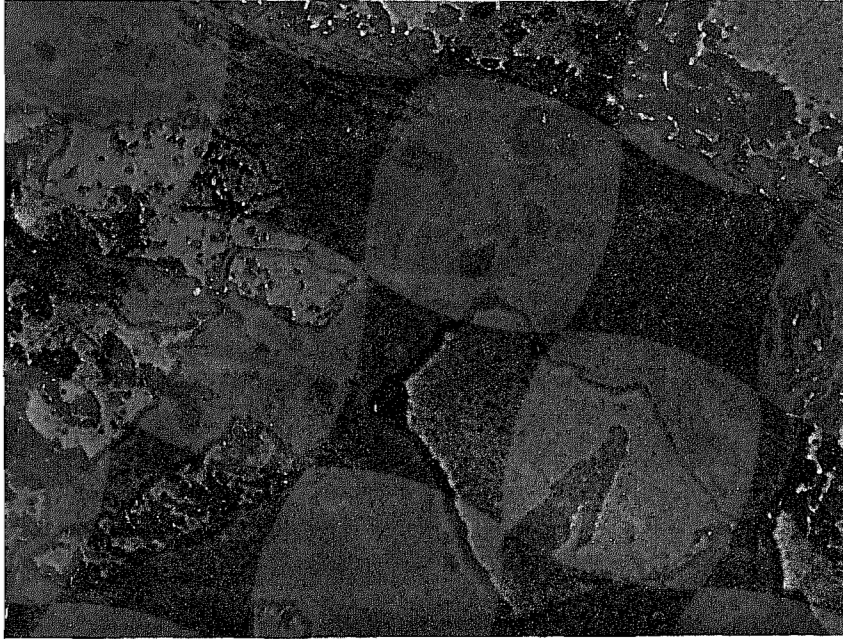
A
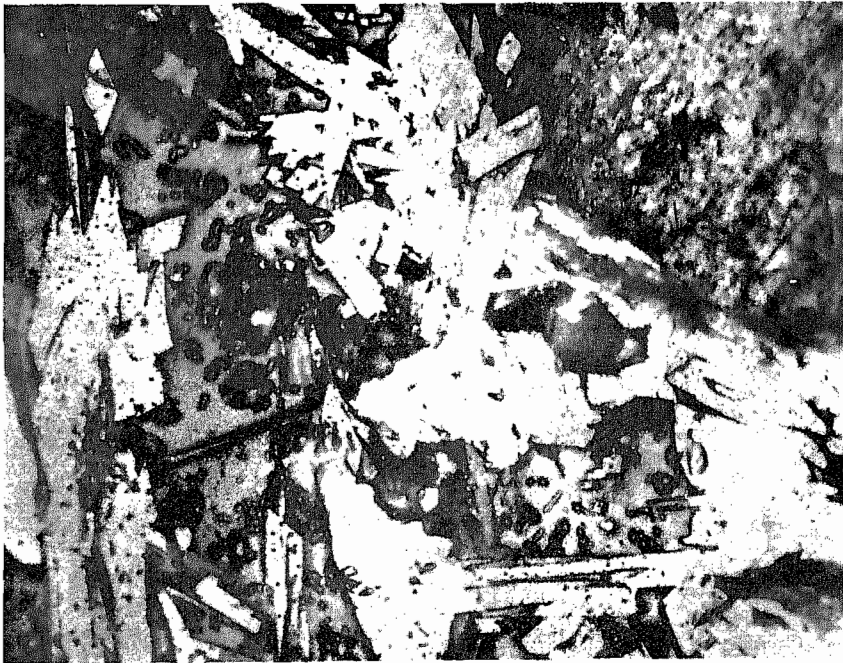
B

Figure D-1. (A) F(0.5) Sample, 7hr. Firing 250X
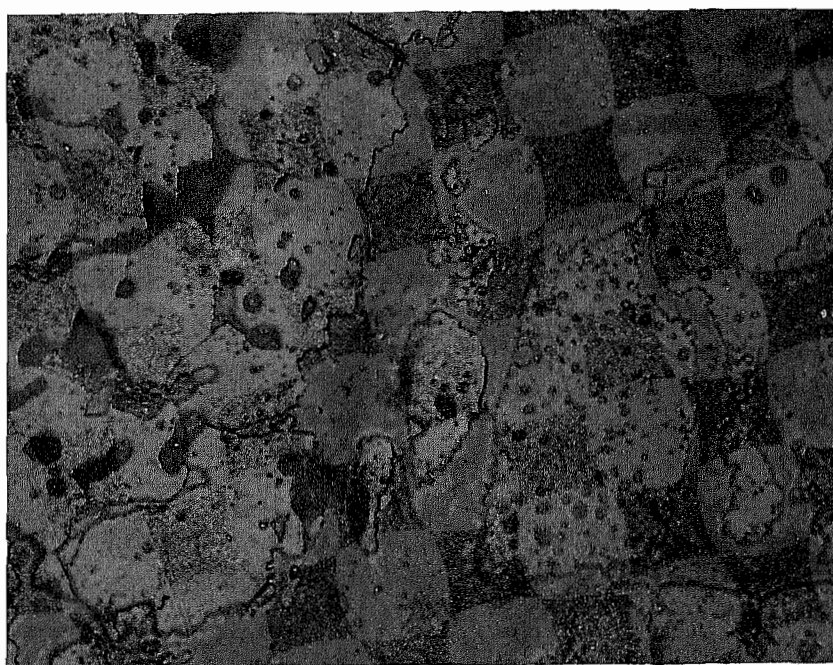(B) F(0.5) Sample, 3hr. Firing 600X
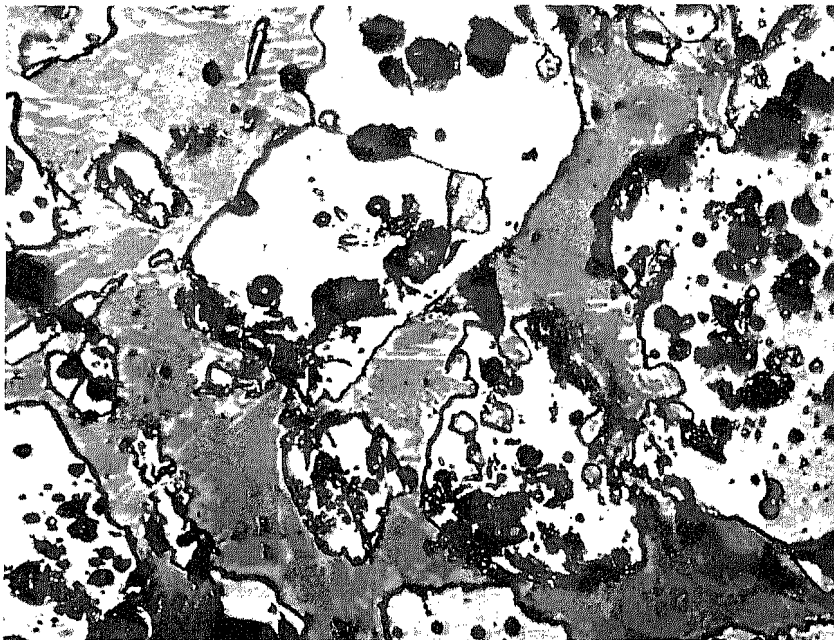
A
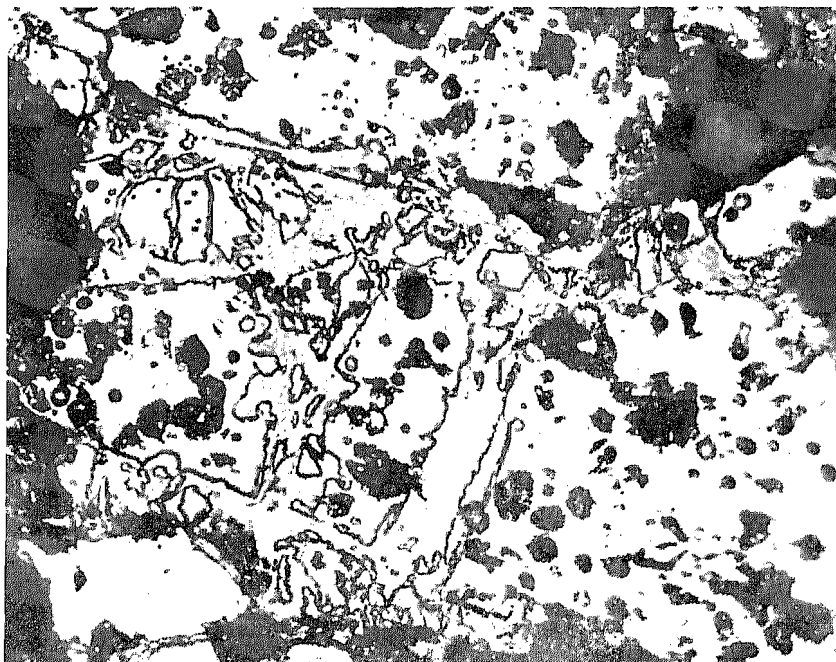
B

Figure D-2. (A) S(0.5) Sample, 3hr. Firing 250X
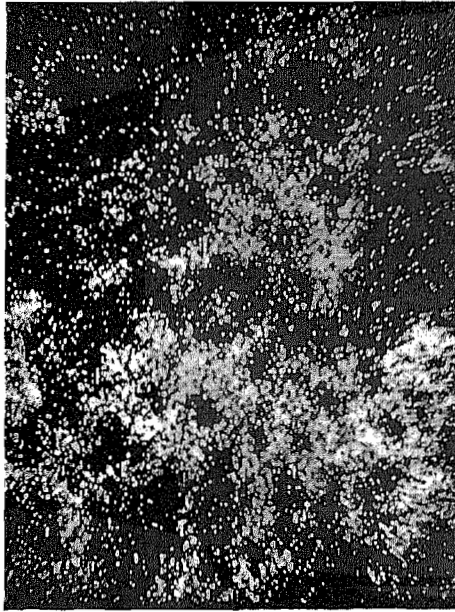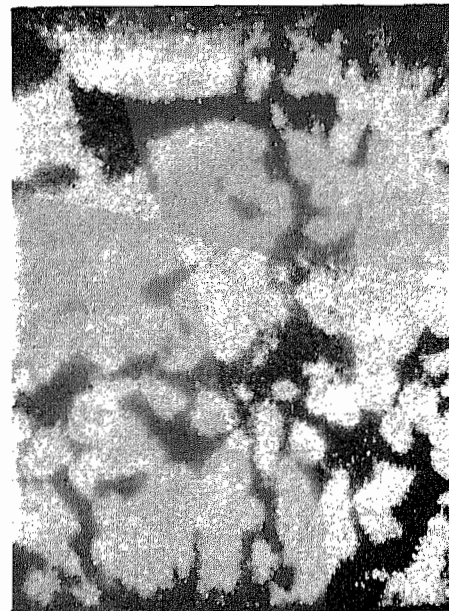(B) S(0.04) Sample, 7hr. Firing 250X
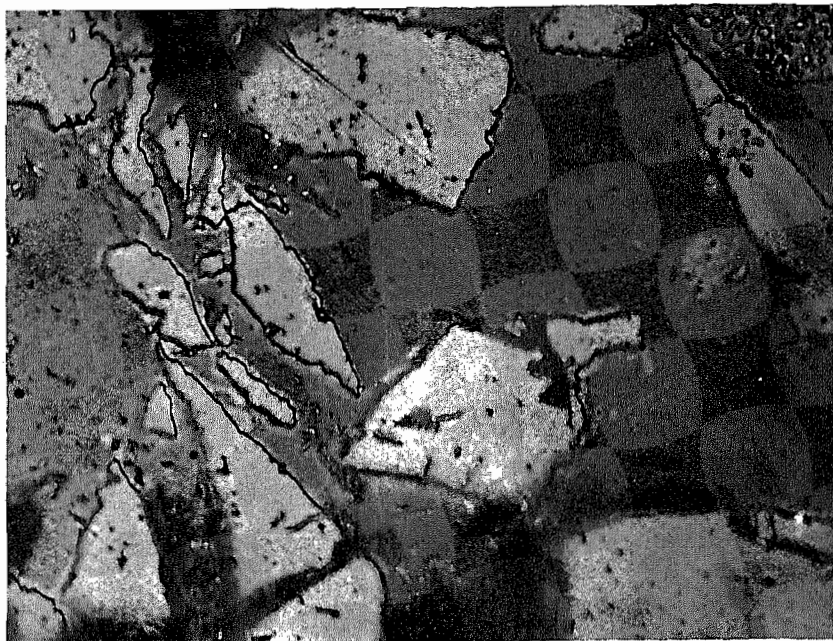
Figure D-3. (A) F(0.07) Sample, 3hr. Firing 250X
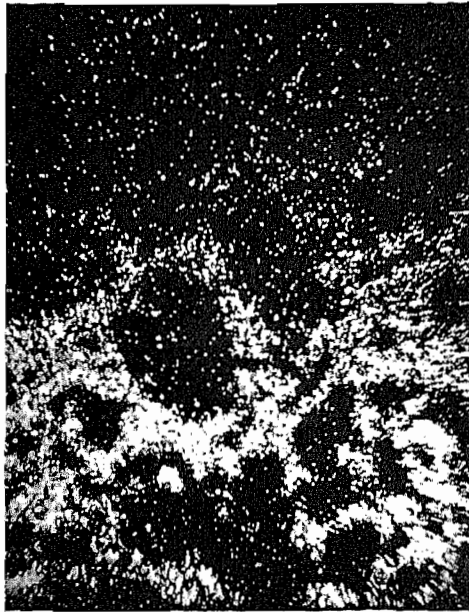   (B) S(0.3) Sample, 3hr. Firing 250X

Si Scan
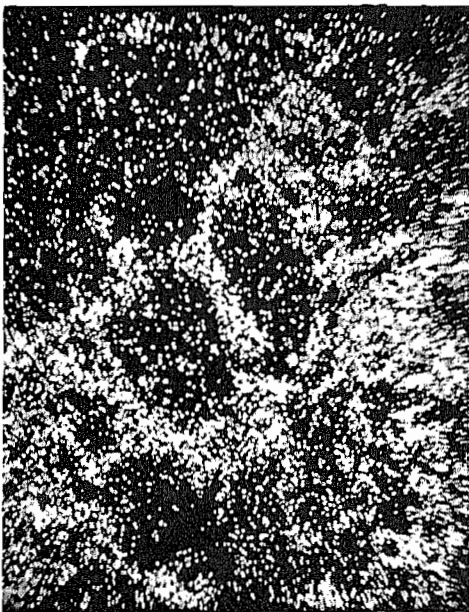
Backscattered
Electron Image

Na Scan

Al Scan

Figure D-4. Electron Probe Microanalysis of
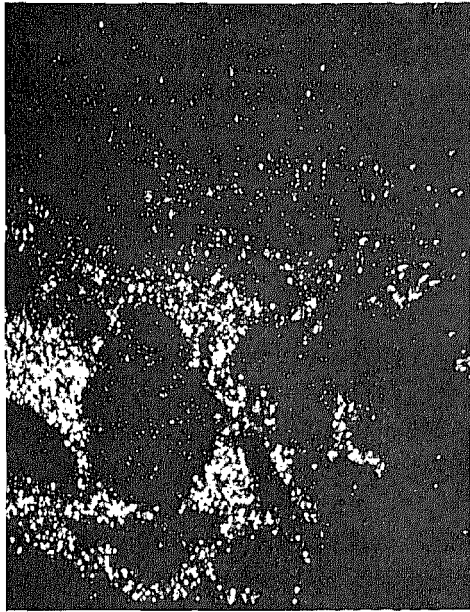S (0.04). Sample, 7 hr. Firing
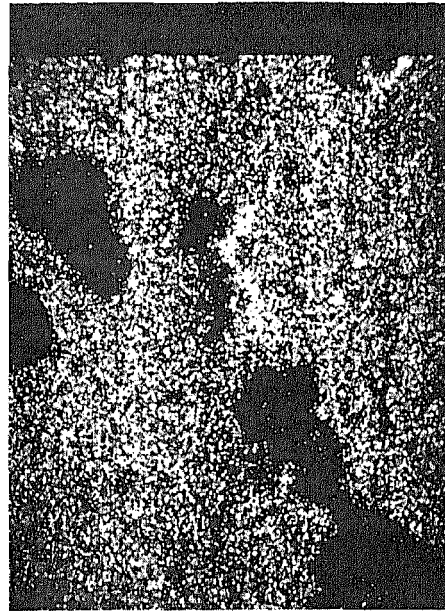
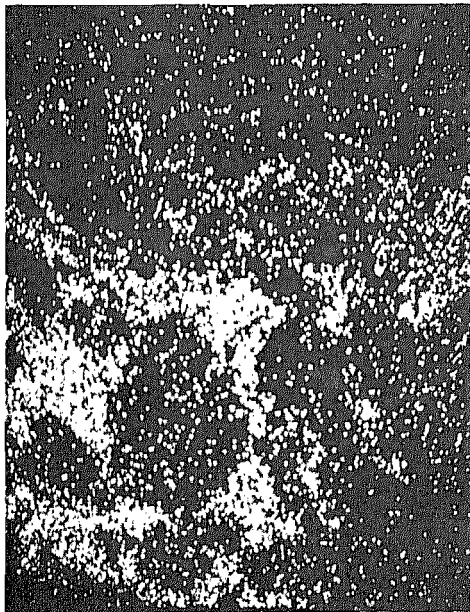Si Scan

Backscattered
Electron Image

Na Scan

Al Scan

Figure D-5. Electron Probe Microanalysis of
S (0.5) Sample, 3 hr. Firing

Si Scan

Backscattered
Electron Image

Na Scan

Al Scan

Figure D-6. Electron Probe Microanalysis of
F (0.5) Sample, 7hr. Firing

APPENDIX E

ERROR ANALYSIS

Random errors in the individual determinations of the
steady state creep rates, Table IV, were estimated by com-
puting the 95% confidence interval for each set of data.
The Student t distribution was used to determine the width
of the confidence interval*. Calculated confidence intervals
are given in Table E-I.

Temperature fluctuations during the control cycle and
gradients within the furnace were considered to be the major
sources of error influencing the precision of the rate meas-
urements.

The error in activation energy due to random error in
creep rates and temperature measurements was obtained by
differentiating the expression for the temperature depend-
ence of the creep rate, equation 3, page 8. Assuming finite
increments in creep rate, Table E-1, and temperature, 5
degrees, a maximum error of 1.1 kcal/mole was obtained.

The major sources of error in the activation energies
were considered to be sample differences and mineralogical
changes in the samples during the creep tests.

*M. G. Natrella, Experimental Statistics, NBS Handbook 91
  Chapter 5, pp 1-46 (1963)

TABLE E-I

CONFIDENCE INTERVALS FOR STEADY STATE CREEP RATES*

Sample	Firing Treatment 1530°C (hours)	Width of 95% Confidence Interval (%/min. X 10^4)			
		1450°C	1480°C	1500°C	1515°C
S(0.04)	7	0.07	0.09	0.15	0.13
F(0.5)	7	0.09	–	0.12	0.20
S(0.04)	3	0.10	0.35	–	0.50
F(0.5)	3	0.20	0.30	–	0.40
S(0.3)	3	–	0.40	0.52, 0.80	0.46
F(0.07)	3	–	0.58	0.87, 0.51	0.57
S(0.5)	3	0.14	0.45	–	–

* See Table IV

VITA

Vernon L. Burdick was born November 4, 1938 at Olean,
New York. He attended public schools in Portville, New
York and graduated from the Portville Central High School in
June, 1956. After one year of employment with the
Worthington Corporation, Wellsville, New York, he enrolled
in the New York State College of Ceramics at Alfred Univer-
sity in September, 1957. In June, 1961 he was granted the
B.S. degree in Ceramic Engineering and continued work toward
the M.S. degree until September, 1963. The M.S. degree was
completed in May, 1965. From September, 1963 until the
present, he attended the graduate school of the University
of Missouri at Rolla studying for the Ph.D. degree in
Ceramic Engineering.